IVYSPRING INTERNATIONAL PUBLISHER

Theranostics

2027; 17(1): 551-572. doi: 10.7150/thno.135792

Research Paper

Continuous generation of functional human iPSC-derived NK cells in a scalable hematopoietic organoid system

Fawaz Saleh[1,2,✉], Lucas Rebuffet[3], Roland Jacobs[4], Agnes Bonifacius[5,7,8], Berislav Čuvalo[6], Edwin Emilio Valdivia Malqui[1], Adrien Mazuel[3], Reinhold Förster[6,7,8], Britta Eiz-Vesper[5,7,8], Greta Meyer[9], Svenja Gaedcke[1,10], Sabine Buyny[4], Dominik Schmiedel[11], Duck Cho[12], Marco Carvalho Oliveira[1], Christine Falk[8,9,10], Adan C. Jirmo[13], Gesine Hansen[1,8,10], Eric Vivier[3,14,15,16], Nico Lachmann[1,2, 8,10,17,✉]

1. Department for Pediatric Pneumology, Allergology and Neonatology, Hannover Medical School, Hannover, 30625, Germany.
2. Regenerative Biology to Reconstructive Therapy (REBIRTH) Center for Translational and Regenerative Medicine, Hannover Medical School, Hannover, 30625, Germany.
3. Aix Marseille Université, CNRS, INSERM, Centre d'Immunologie de Marseille-Luminy, Marseille, France.
4. Department of Rheumatology and Clinical Immunology, Hannover Medical School, Hannover, Germany.
5. Institute for Transfusion Medicine and Transplant Engineering, Hannover Medical School, Hannover, Germany.
6. Institute of Immunology, Hannover Medical School, Hannover, Germany.
7. German Center for Infection Research (DZIF), Partner Site Hannover-Braunschweig, 30625 Hannover, Germany.
8. Cluster of Excellence RESIST (EXC2155), Hannover Medical School, Hannover, 30625, Germany.
9. Institute of Transplant Immunology, Hannover Medical School, Hannover, Germany.
10. Biomedical Research in Endstage and Obstructive Lung Disease Hannover (BREATH), German Center for Lung Research (DZL), Hannover, Germany.
11. Fraunhofer Institute for Cell Therapy and Immunology (IZI), Leipzig, Germany.
12. Department of Laboratory Medicine and Genetics, Samsung Medical Center, SungKyunkwan University School of Medicine, Seoul, Korea.
13. Department of Pediatric Surgery, Hannover Medical School, Hannover, Germany.
14. Innate Pharma Research Laboratories, Innate Pharma, Marseille, France.
15. APHM, Hôpital de la Timone, Marseille-Immunopole Profiling Platform, Marseille, France.
16. Paris Saclay Cancer Cluster, Villejuif, France; Université Paris-Saclay, Gustave Roussy, INSERM, Next-generation immuno-oncology research and therapy in pediatric and adult cancer, Villejuif, France.
17. Fraunhofer Institute for Toxicology and Experimental Medicine (ITEM), Hannover, Germany.

✉ Corresponding authors: Prof. Dr. Nico Lachmann, Hannover Medical School, Department for Pediatric Pneumology, Allergology and Neonatology, Carl-Neuberg-Str. 1, 30625 Hannover, Germany, eMail: lachmann.nico@mh-hannover.de. Dr. Fawaz Saleh, Hannover Medical School, Department for Pediatric Pneumology, Allergology and Neonatology, Carl-Neuberg-Str. 1, 30625 Hannover, Germany, eMail: saleh.fawaz@mh-hannover.de.

© 2027 The Author(s). This is an open access article distributed under the Creative Commons Attribution 4.0 International Licence, subject to the Publisher's Terms of Use at https://ivyspring.com/terms.

Received: 2026.04.07; Accepted: 2026.09.22; Published: 2027.01.01

Abstract

Rationale: Induced pluripotent stem cell (iPSC)-derived natural killer (iNK) cells offer an off-the-shelf platform for cancer immunotherapy, but scalable production and consistent functionality remain key challenges. Deeper analytical and bioprocess insights into scalable manufacturing is needed to improve the quality, consistency, and affordability of cell products. Here we aimed to develop and characterize a scalable bioprocess for the continuous generation of functional iNK cells preserving their phenotypic, transcriptional, and functional properties across scales.

Methods: Guided mesodermal induction followed by cytokine-driven hematopoietic specification was used to differentiate iPSCs into iNK cells in small-scale (3 mL plates) and moderate-scale (50 mL) bioreactors. Phenotypic characterization, transcriptional profiling, functional cytotoxicity assays, cytokine secretion, degranulation, and migration analyses were performed to evaluate scalability, stability, and functionality.

Results: The scalable bioprocess enabled continuous generation of phenotypically stable iNK cell intermediates with emerging functional properties across both production scales. Differentiation yielded $CD45^+CD3^-CD7^+CD56^{+/-}$ iNK subsets with dynamic surface-marker expression and reproducible yields, achieving approximately 50-fold amplification per input iPSC. Phenotypic and functional stability was maintained without scale-dependent differences in iNK subset composition or receptor expression, including KIR profiles. Differentiation generated transcriptionally distinct iNK populations, whereas expansion preferentially enriched $CD56^+$ subsets and increased expression of activating receptors (DNAM-1 and NKG2D), alongside dynamic regulation of inhibitory receptors. The resulting iNK cell populations displayed heterogeneous developmental states with transcriptional programs resembling primary NK cells, including activation-associated and cytokine-induced memory-like signatures. Bioreactor-

based production supported sustained sequential harvests without compromising phenotype, cytotoxic function, or subset diversity. Expanded iNK cells demonstrated enhanced lytic activity, target-cell apoptosis, degranulation, secretion of cytolytic effector molecules comparable to expanded primary NK cells, and migratory behavior similar to donor-derived peripheral blood NK cells.

Conclusions: This bioprocess establishes continuous and scalable platform for manufacturing iNK cells that preserves phenotypic diversity, transcriptional complexity, and functional competence across production scales, supporting robust and cost-effective production of next-generation cell-based immunotherapies.

Keywords: organoids, haematopoiesis, hiPSC, natural killer cells, up-scaling, bioreactor, regenerative medicine, bioprocessing, cell manufacturing

Introduction

Natural killer (NK) cells are cytotoxic innate lymphocytes with established roles in tumor surveillance and antiviral defense [1, 2]. Their intrinsic cytotoxicity, cytokine production, and capacity for antibody-dependent cellular cytotoxicity [1, 3-6] have positioned them as a promising platform for cell-based immunotherapies. Clinical studies have demonstrated both favorable safety profiles and preliminary evidence of anti-tumor activity, supported further by their suitability for allogeneic use [7-9]. NK cells undergo a unique education process that enables them to distinguish self from non-self without any prior sensitization [10-13]. Unlike T cells, NK cells lack T cell receptors (TCRs) and instead rely on germline-encoded activating and inhibitory receptors to recognize stress-induced ligands, cytokine cues, and antibody-opsonized targets [6]. Together, these properties highlight the importance of defining the developmental pathways that establish NK cell identity and effector competence for therapeutic translation.

Given these unique cellular attributes, NK cells have demonstrated clinical promise, and recent clinical development has expanded [14]. However, broader clinical translation and large-scale deployment remain constrained by donor dependence, inter-donor variability, intrinsic heterogeneity among NK sub-populations [15], limited persistence and trafficking. In fact, human induced pluripotent stem cells (hiPSCs) have emerged as a renewable and genetically tractable cell sourcing platform capable of addressing many of these limitations [16-18]. iPSCs support standardized and scalable production [19-21] of immune cells and provide an experimentally accessible system for dissecting human hematopoietic [21-24] and lymphoid development [25], enabling off-the-shelf immunotherapies while simultaneously offering a controlled platform to investigate human hematopoietic and immune cell ontogeny [18]. However, a limited understanding of the transcriptional and developmental mechanisms governing NK specification from human iPSC-derived progenitors continues to hinder optimization of iPSC-derived NK (iNK) cell manufacturing workflows, many of which remain dependent on feeder layers or static culture formats that constrain manufacturing scalability, reproducibility, and standardization [26, 27].

Consistent with advances in cell engineering, the clinical evaluation of primary NK cell- and iPSC-derived NK cell-based therapies has expanded rapidly. Multiple Phase I and early Phase II trials are currently evaluating safety and preliminary efficacy across hematologic and solid malignancies. For example, FT500 (NCT03841110), the first iPSC-derived NK cell product tested in humans, demonstrated a clinically acceptable safety profile without dose-limiting toxicities in patients with advanced solid tumors. FT516 (NCT04023071), engineered to express a high-affinity, non-cleavable CD16 receptor, achieved objective response rates of approximately 58% in relapsed or refractory B-cell lymphoma [28]. Similarly, FT596 (NCT04245722), a CD19-directed CAR-iPSC-derived NK cell product incorporating IL-15 signaling support, reported overall response rates ranging from 54-75% at higher dose levels in B-cell lymphoma [28]. Additional ongoing studies include CNTY-101 (NCT05336409) targeting CD19-positive B-cell malignancies and FT576 (NCT05182073), a BCMA-directed CAR-iPSC-derived NK cell therapy under evaluation in multiple myeloma. Collectively, these data demonstrate manageable safety profiles and encouraging anti-tumor activity, particularly in hematologic malignancies. Nevertheless, limited *in vivo* persistence and reduced efficacy in solid tumor settings, and challenges associated with scalable, standardized manufacturing [29] remain key challenges to broader clinical implementation.

To address these manufacturing challenges, mechanistically informed scalable differentiation platforms are needed that can resolve NK lineage specification while supporting industrially relevant production. Previous iPSC-derived NK cell platforms recapitulate hematopoietic and early lymphoid intermediates through cytokine-driven protocols commonly centered on IL-3, FLT3L, SCF, IL-7, and IL-15, but many of these approaches rely on feeder-

dependent or static culture systems that constrain scalability and standardization. Moreover, the resulting iNK cell products are typically defined by CD56 expression with only partial acquisition of KIRs and other maturation markers, resembling $CD56^{bright}$, immature NK subsets rather than fully educated $CD56^{dim}$, KIR-diverse peripheral blood NK cells. Together, these developmental and bioprocessing limitations restrict scalability and product consistency, underscoring the need for next-generation, bioreactor-compatible differentiation systems that are more closely aligned with *in vivo* NK ontogeny.

Building on our previously established hematopoietic organoid (hemanoid) platform[30], which enables the generation of hematopoietic progenitors from single-cell human iPSCs through simultaneous mesoderm induction and three-dimensional self-aggregation, we sought to exploit the developmental plasticity of this system for NK cell specification. In this platform, mesoderm-primed hemanoids recapitulate key aspects of early developmental hematopoiesis [31]. and provide a controllable microenvironment in which hematopoietic lineage commitment can be directed through defined cytokine cues. We previously demonstrated that modification of the cytokine milieu following mesoderm induction redirects hematopoietic progenitors toward the macrophage lineage through supplementation with M-CSF [30-32]. These findings suggest that the hemanoid platform represents a versatile developmental intermediate from which alternative hematopoietic lineages can be generated by rational modulation of lineage-specifying signals. Accordingly, in the present study, we investigated whether sequential supplementation with SCF, FLT3L, IL-3, IL-7, and IL-15 could similarly direct hematopoietic progenitors toward the NK lineage within the organoid microenvironment. As iNK cells emerge, they are released from the hemanoid into the surrounding culture, enabling continuous harvest and downstream expansion. This developmental strategy combines organoid-based recapitulation of hematopoiesis with a scalable manufacturing concept for the generation of functional iNK cells.

In this study, we aimed to develop and evaluate a novel manufacturing strategy for iPSC-derived NK cells. Focusing on scalable culture configurations, we assessed continuous hematopoietic and NK cell generation using a hematopoietic organoid-based system and compared small-scale (3 mL plates) adherent and suspension formats. Finally, we translated these findings into moderate-scale production by implementing a 50 mL benchtop bioreactor platform, thereby linking developmental optimization with scalable bioprocess design.

Materials and Methods

Experimental model and study participant details

Cell culture

All cells in this study were in standard incubator conditions (20% O_2, 5% CO_2, and 37 ^oC).

Human pluripotent stem cell cultivation

The human pluripotent stem cell line used in this study were obtained with full ethical approval and validated using standard methods including chromosomal analysis, pluripotency and absence of plasmid integration. Experiments were conducted utilizing human induced pluripotent stem cell line LiPSC-GR1.1, generated by Lonza under the auspices of the National Institutes of Health (NIH) [33] (https://hpscreg.eu/cell-line/RUCDRi002-A). All experimental details involving the generation of this CGMP grade iPSC line are described by Baghbaderani et al [33]. hiPSCs expansion was performed in feeder-free monolayer culture on Geltrex™ or vitronectin coated plates (following manufactures recommendations). hiPSCs were maintained in an incubator at 37 ^oC with 5 % CO_2. For passaging, cells were pre-washed with PBS without Ca^{2+}/Mg^{2+} and detached with Accutase® (Sigma-Aldrich) for 3-5 min. Subsequently, Accutase® was diluted with PBS without Ca^{2+}/Mg^{2+}, cell solution was transferred into a conical tube and centrifuged at 300 x g for 3 min. The cell pellet was reconstituted in Essential (E8) medium [34] supplemented with 10 mM Y-27632 (TOCRIS), referred to as E8 + RI. The cells were inoculated in E8 + RI and the medium was exchanged after 48 h (day 2). The cells were passaged after 72 h (day 3) for a maximum of 6 passages (see Table S1 key resources, in supplemental information).

Generation of hematopoietic organoids

For this study, hematopoietic organoids also known as hemanoids were generated following the previously published protocol in the benchtop bioreactor [30] and in 6 well plates. In brief, human iPSCs were used as starting material. In the first step, iPSCs were obtained in a single-cell solution in a 6-well plate and transferred onto an orbital shaker set at 70 rpm to induce aggregation and mesoderm induction simultaneously, using 18 mL mesoderm media 1a (E8 medium + hVEGF 50 ng/mL + hBMP4 50 ng/mL + hSCF 20 ng/mL + 10 mM Y-27632 (RI)). After 24 h, a full media change was performed using mesoderm media 1b (E6 medium + hVEGF 50 ng/mL + hBMP4 50 ng/mL + hSCF 20 ng/mL + (RI)), and the orbital

shaker speed was increased to 85 rpm. On days 4 and 7, 18 mL full media changes were performed using mesoderm media 2 (E6 medium + IL3 25 ng/mL + hVEGF 50 ng/mL + hBMP4 50 ng/mL + hSCF 20 ng/mL + (RI)). On day 10, hematopoietic organoids were ready for hematopoietic differentiation toward Natural killer (NK) cell fate.

Generation of hiPSC-derived natural killer (iNK) cells

To induce iNK cell fate, we adopted from previously published protocol[35], with minor adjustments to accommodate our hematopoietic organoid system, which entailed Xvivo-15 (Lonza) + 1% penicillin-streptomycin (Gibco) + 2 mM L-glutamine (Invitrogen) + 0.05 mM b-mercaptoethanol (Invitrogen) + IL3 5 ng/mL + hSCF 20 ng/mL + IL7 20 ng/mL + FLT3 10 ng/mL + IL15 10 ng/mL + RI (for the first week). The aggregates were used in adherent and suspension-based cultures by simply transferring the organoids into the respective cell culture plate. For adherent cultures, the plates were coated with 0.1% gelatin to support the attachment of the aggregates. Half medium changes were performed twice in the first week and once every 5-7 days for the continuous production of iPSC-derived Natural killer cells. Cells were harvested on week 4, week 6, week 8, week 10 and annotated as Harvest 1, 2, 3 and 4, respectively and used for all subsequent experiments. In the small-scale (3 mL) culture plates, organoids remained productive across all four harvests. In contrast, in the moderate-scale (50 mL) bioreactor cultures, iNK cell output declined earlier, and productive release ceased after the third harvest; therefore, only three harvests were performed under these conditions. The iNK cells used throughout this study were not pooled across harvests. Each harvest (weeks 4, 6, 8, and 10; Harvests 1-4) was analyzed individually and used independently for all downstream experiments.

Flow cytometry

Flow cytometry analysis was performed on the different natural killer cell populations and hematopoietic organoids. The hemanoids were prepared as previously mentioned[30, 31]. Cells were treated PBS + FCR blocking agent (1:100, Miltenyi #130-059-901) + viability dye (Zombie Aqua fixable viability kit, BioLegend) was used following the manufacturer´s recommendation, which was added prior to antibody staining. Staining was performed on ice for 30 min in the dark (see Table S2 NK cell characterization in supplemental information). Cells were washed and acquired with FACS buffer (PBS + 2 mM EDTA + 5% FCS). Acquisition was performed by flow cytometry using the CytoflexS (Beckman Coulter) or LSR. Single stained sample controls were used for compensation for multicolor staining. Analysis of the data was performed using FlowJo software (BD Bioscience).

hiPSC-derived natural killer cell expansion

All cells produced from each harvest were expanded directly and co-cultured with 60-Gy γ-irradiated K562-OX40L-mbIL-18/-21 feeder cells at a cell-to-feeder ratio of 6:1. The cells were inoculated in 24-well adherent plate with 2 mL/ well of NK expansion media (Xpander basal, supplement (50x), 5% Human AB sera, 1% Glutamax (Gibco), 0.1% b-mercaptoethanol, 1% penicillin-streptomycin (Gibco)) + IL2 20 IU/mL for the first week, half media changes were performed every other day and final concentration was maintained at 20 IU/mL of IL2. After 7 days the cells were collected and split, if cell count of one well was more than 4×10^6 cells, they were split at a ratio of 1:4 if less than 4×10^6, cells were split at a ratio 1:2. Cells were inoculated at a density 1-1.5 x 10^6 cells/well in fresh NK expansion media + IL2 100 IU/mL + IL15 20 ng/mL, half media changes were performed every other day and final concentration was maintained at 100U/mL of IL2 and 20 ng/mL IL-15. The same was performed for day 14.

CD107a degranulation assay

iNK cells were incubated with or without 5×10^3 target cells (K562) at ratio of (effector:target) 2:1, 5:1 and iNK cells without target cells in a 96 flat bottom plate in triplicate wells. Monensin was added after 1 h of co-culture, and the plate was incubated for an additional 4 h. After 4 h, iNK cells were collected and stained with anti-human CD3, CD56, CD16, CD107a. Specific degranulation was calculated by subtracting the basal CD107a expression observed in iNK cells cultured without target cells from the CD107a expression measured in the presence of target cells.

^{51}Cr release assay

Standard ^{51}Chromium (^{51}Cr) release cytotoxicity assays were performed using human K562 cell line (German Collection of Microorganisms and Cell Cultures, DMSZ, Braunschweig, Germany) as targets [36]. K562 cells (2×10^6) were labeled with 3 MBq $Na_2{}^{51}CrO_4$ (Hartmann, Braunschweig, Germany) for 1 h and washed three times. After three washes, target cells (5×10^3/50 µL) were seeded into 96 well V-bottom plates. Effector cells (iPSC-NK cells) were added in defined effector to target (E/T) cell ratios (5:1 and 2:1). For determining spontaneous and maximum ^{51}Cr release cells were incubated with media alone or lysed by adding 1% Triton X-100 (Sigma, St. Louis, MO, USA), respectively. All tests were performed in triplicates. To improve the contact between effector

and target cells, plates were gently centrifuged for 3 min. at 100 g. After 4 h of incubation at 37 °C and subsequent centrifugation for 5 min at 300 g aliquots of cell-free supernatants were harvested. Released ^{51}Cr was measured by using a Microbeta 1450 counter (Perkin Elmer, Rodgau-Jügesheim, Germany). Specific lysis was calculated using following formula: [(experimental release – spontaneous release) / (release maximum – spontaneous release)] x 100. To facilitate quantitative comparison of cytotoxic activity between experimental groups, cytotoxicity data were additionally expressed as lytic units (LU), calculated according to the method described by Bryant et al. [37] and Chatterjee et al. [38]. Lytic units normalize cytotoxic activity to the number of effector cells required to achieve a defined level of target-cell lysis, thereby providing a standardized measure of NK cell cytotoxic function across experimental conditions.

iPSC-NK cell induced apoptosis assessment of K562

iPSC-NK cells were labeled with anti-human CD45 PE (Biolegend cat #304008) and co-cultured with K562 at a ratio 5:1, Apoptosis dye (Caspases3/7, Sartorius part: 4440; Annexin V, Sartorius part: 4642) was added prior to the start of the experiment. Images were collected over the span of 48 h and GFP intensity was measured using Incucyte® S3 Live-Cell Analysis Instrument.

Cytospin staining

For cytospin staining, 2×10^4 or 3×10^4 cells were centrifuged on glass slides using a Cytofuge® (Medite) at 700 rpm for 10 min. The slides were left to air-dry, and were stained with 0.25% (w/v) of May-Grünwald solution (Roth) for 5 min and washed three times with distilled water. The second staining round was performed using 5% GIEMSA solution (Roth) for 20 min. Afterwards the slides were thoroughly washed three times with distilled water. Stained and air-dried cells were fixed with ROTI®Histokitt mounting solution (Roth) and imaged using Olympus BX41 microscope.

Isolation and expansion of primary NK cells

Primary NK cells were isolated from residual blood samples of platelet donors at the Institute of Transfusion Medicine and Transplant Engineering, Hannover Medical School. Written informed consent was acquired from all donors, and the study was approved by the Institutional Review Board of Hannover Medical School on the basis of the declaration of Helsinki (ethics votes: 3639-2017). In brief, PBMCs were isolated via density gradient centrifugation, followed by isolation of primary NK cells using the NK Cell Isolation Kit, human (Miltenyi Biotec) according to the manufacturer's instructions. Purity of the obtained cell fractions were evaluated by flow cytometry using anti-CD45 AF700, anti-CD3 FITC, anti-CD56 PE and anti-CD16 APC-Cy7 (BioLegend). Samples were acquired on a FACS Canto 10c system (BD Biosciences). NK cell expansion was performed using the NK Cell Activation/Expansion Kit, human (Miltenyi Biotec) according to the manufacturer's instructions. For assessment of the cytokine profile, culture supernatants were collected daily and stored at -20 °C until further use.

Cytokine profile

Concentrations of effector molecules in cell culture supernatants were determined by LEGENDPlex™ using the Human CD8/NK Cell Kit (BioLegend) according to the manufacturer's instructions. Samples were acquired on a FACS Symphony system (BD Biosciences) and data analysis was performed using the LEGENDPlex™ Software.

Human precision-cut lung slices (PCLS)

Human precision-cut lung slices (PCLS) were prepared from tumor-free lung tissue obtained from patients undergoing lobectomy for lung cancer at Hannover Medical School and will be described in detail elsewhere. In short, healthy tissue regions distal to the tumor were processed into 500 µm-thick slices using a McIlwain Tissue Chopper. Following preparation, PCLS were washed in RPMI-1640 medium, cryopreserved in freezing medium using a controlled-rate freezing container (Mr. Frosty, Thermo Fisher Scientific), and stored at -80 °C until use. High-resolution HLA class I and class II typing was performed using next-generation sequencing. For the co-culture experiments, the lung tissue donor and the third-party peripheral blood donor were partially HLA-matched, sharing one allele each at the HLA-A, HLA-B, and HLA-C loci, whereas HLA-DRB1 and HLA-DQB1 alleles were mismatched (Table S3). All patient samples, or their next of kin, provided full informed consent. Experiments were approved by the Local Ethics Committee in accordance with the world medical association's international code of ethics (10351_B0_K_2022).

Live-cell imaging of NK cell migration

Cryopreserved PCLS were thawed one day prior to infection and cultured in 24-well plates containing RPMI-1640 supplemented with 2 mM L-glutamine, 100 IU/mL penicillin/streptomycin (Gibco), and 0.05 mM β-mercaptoethanol (Sigma-Aldrich). Individual PCLS were infected with 1×10^5 PFU RV-TB40-BACKL7-SE-EGFP-ΔUS2-6+ΔUS11-UL40rep in 100 µL PBS for 3 h. Subsequently, culture medium was added

to a final volume of 500 µL per well and replaced daily. All incubations were performed on a 3D Sunflower Mini-Shaker (Biosan) at 5 rpm under standard cell culture conditions.

NK cells were isolated from PBMCs using the untouched NK Cell Isolation Kit, (Miltenyi Biotec), and expanded according to the manufacturer's instructions for 13 days before use for the experiments. Prior to co-culture, pNK cells and iNK cells were stained with SPY650 DNA (Spirochrome) and CellBrite Steady 550 Membrane Stain (Biotium) in serum-free RPMI-1640 medium for 15 min at 37°C. Cells were washed, allowed to recover for 4-6 h in complete human NK medium, washed again, and cultured overnight (12 h) at a density of 2×10^6 cells/mL.

For migration analysis, one HCMV-infected PCLS (day 3 post-infection) was transferred into a 48-well plate, before 1×10^6 labeled NK cells were added on top and co-cultured for 30 min at 37 °C under standard cell culture conditions. Following co-culture, PCLS were immediately transferred into a custom-built imaging chamber filled with CO_2-independent imaging medium supplemented with 2 mM L-glutamine, 100 IU/mL penicillin/streptomycin (Gibco), 0.05 mM β-mercaptoethanol (Sigma-Aldrich), and 3.2 g/L D-glucose (Gibco). The chamber was maintained at 37 °C throughout image acquisition.

Two-photon microscopy

Time-lapse imaging was performed using a TriM Scope modular two-photon microscope (LaVision BioTec) equipped with an Olympus upright microscope and a W Plan-Apochromat 20×/1.0 water-immersion objective (Zeiss). Excitation was achieved using a Mai Tai DeepSee laser (Spectra-Physics) tuned to 910 nm for GFP and second-harmonic generation or an InSight DeepSee laser (Spectra-Physics) tuned to 1105 nm. For human PCLS, mage stacks comprising up to 34 optical sections were acquired using the 20× objective over a lateral field of view of 450 × 450 µm and a z-depth ranging from 100 to 200 µm. Time-lapse images were acquired at 30 or 60 s intervals. Image processing and analysis were performed using Imaris 10.1 (Bitplane). Median filtering for noise reduction and drift correction was applied when required. Cell tracking was performed using the autoregressive motion algorithm in Imaris with an estimated cell diameter of 12 µm, a maximum tracking distance of 10 µm, and a gap size of three frames. Tracks were manually inspected, corrected where necessary, and filtered for a minimum track duration of 2 min. Time-lapse recordings were acquired at either 30 s or 60 s intervals. To enable direct comparison between datasets, acceleration values obtained from recordings acquired at 30 s intervals were adjusted by a factor of two in Microsoft Excel prior to statistical analysis. All remaining migration parameters were analyzed as exported from Imaris.

Single-cell RNA-seq analysis:

Sample preparation:

Human iPSC-NK cells derived before and after expansion were harvested. Viable cells were purified by fluorescence activated cell sorting (FACS) on basis of scatter properties and inclusion of Calcien positive events, which has been added before sorting as per manufacturers recommendations (Thermofisher).

Library preparation and sequencing

Library generation:

Library preparation for single cell mRNA-Seq analysis was performed according to the Chromium NextGEM Single Cell 3' Reagent Kits v3.1 User Guide (Manual Part Number CG000204 Rev B; 10x Genomics). According to the protocol, a given excess of cells was loaded to the 10x controller in order to reach a target number of 4,000 cells per sample. Fragment length distribution of generated libraries was monitored using 'Bioanalyzer High Sensitivity DNA Assay' (5067-4626; Agilent Technologies). Quantification of libraries was performed by use of the 'Qubit® dsDNA HS Assay Kit' (ThermoFisher Scientific #Q32854).

Sequencing run:

Equal molar proportions of generated mRNA expression libraries (constituting 20% of sequencing run capacity each) were pooled accordingly, denatured with NaOH, and were finally diluted to 1.8 pM according to the 'Denature and Dilute Libraries Guide' (Illumina, Document #15048776 v02). 1.3 mL of denatured pool (including 1% PhiX) was sequenced on an Illumina NextSeq500 sequencer using one high-output flowcell for 75 cycles and 400 million clusters (Illumina #20024906). Sequencing was performed according to the following settings: 28 bp as sequence read 1; 56 bp as sequence read 2; 8 bp as index read 1; no index read 2.

Raw data processing:

The 10x Genomics CellRanger analysis pipeline set (v7.1.0) was used with default parameters. Briefly, BCL files were demultiplexed into FASTQ files by cellranger mkfastq using the respective sample sheet with utilized 10x barcodes. The cellranger count pipeline was used to align read data to the reference genome provided by 10x Genomics (Human reference dataset refdata-gex-GRCh38-2020-A), counting

aligned reads per gene, and calculating clustering and summary statistics. Subsequently, outputs from cellranger count of all samples were aggregated, normalized to the same sequencing depth, and then the feature-barcode matrices were recomputed by cellranger aggr.

Finally, the Loupe Cell Browser (10x Genomics) was utilized to view and revise annotated clusters, based on the implemented tSNE or UMAP algorithms.

Bioinformatic analysis of single cell sequencing data

Single-cell RNA-seq data processing and dimensionality reduction

Raw single-cell RNA sequencing (scRNA-seq) data were processed and analyzed using Seurat (v4.0.0). Gene expression matrices were log-normalized using a global-scaling normalization method. The top 2,000 highly variable genes were selected for downstream analysis based on variance-stabilizing transformation. Prior to dimensionality reduction, data were scaled and centered; during this step, cell cycle phase scores were calculated for each cell using the CellCycleScoring function within Seurat to identify proliferation phases. Principal Component Analysis (PCA) was performed on the scaled data, utilizing the top 50 principal components (PCs) to construct a Shared Nearest Neighbor (SNN) graph. Non-linear dimensional reduction and visualization were achieved using Uniform Manifold Approximation and Projection (UMAP). Clusters were identified using the graph-based modularity optimization algorithm implemented in the FindClusters function. The resulting UMAP embeddings served as the common reference for all downstream analyses. Functional scoring and cell-type annotation were projected onto these existing embeddings to characterize the developmental identity of each cluster rather than to generate new cluster assignments.

Differential expression and marker identification

To identify cluster-specific marker genes, differential expression analysis was performed using the FindAllMarkers function in Seurat. Statistical significance was assessed using the Wilcoxon Rank Sum test (method = 'wilcox'). Markers were defined as genes showing a positive fold change (only.pos = TRUE) with a minimum natural log fold-change threshold of 0.25 (logfc.threshold = 0.25) and expressed in at least 20% of cells within either of the two groups tested (min.pct = 0.2).

Functional scoring and signature analysis

Cellular scoring for specific functional signatures was computed using the AddModuleScore function. For general cluster characterization, scores were generated using the top 20 cluster-specific markers identified as described above. To determine the developmental identity of the generated iNK populations, published gene signatures representing distinct stages of NK cell differentiation were projected onto the common UMAP embedding. These module scores were used to annotate clusters according to their developmental state and to distinguish NK progenitor-like cells, intermediate NK cell populations, and mature NK cell states.

Additionally, specific NK cell states were interrogated using established gene signatures:

- NK scoring: Cells were scored against a reference of NKs and NK progenitors signature derived from [39] to assess overall commitment to the NK cell lineage.
- NK progenitor score: Cells were scored against published NK progenitor signatures derived from [40] to identify progenitor-like intermediates within the differentiation trajectory.
- Crinier 13 score (Mature NK): A signature comprising 13 human NK-specific genes extracted from [40] was applied to identify transcriptionally mature NK cell populations and distinguish them from less differentiated intermediates.

Automated cell classification

For the precise identification of effector memory-like (eML) populations, a pre-trained machine learning classifier developed by Foltz et al. [41] was utilized. This classifier stratified cells into four distinct categories: $CD56^{Bright}$, $CD56^{dim}$, eML1, and eML2. This reference-based classification served as an independent validation of the developmental states inferred from the module scoring analyses and enabled comparison of the generated iNK populations with established primary NK cell subsets. The specific code and Docker environment used to reproduce this classification are available at https://zenodo.org/communities/finding_eml/.

Visualization and software specifications

Heatmaps were generated to visualize major NK molecular features using ComplexHeatmap (v2.6.2). To ensure robust visualization, genes were included only if their expression was detected in more than 5% of circulating NK cells. Z-scores were computed for expression levels across the four identified NK cell subpopulations to highlight relative expression differences beyond previously established markers. All analyses were performed in R. Additional R

packages utilized for data handling, annotation [42], and functional profiling included SingleR (v1.4.1) and clusterProfiler (v3.18.1).

PAGA plot analysis

The analysis was performed using Scanpy (v1.8.2, Python 3.9.7). Cells with >25% mitochondrial counts or >6,700 detected genes were removed. Genes expressed in fewer than 2 cells and cells with fewer than 2 total counts were also excluded. Doublets were identified with Scrublet run separately on each sample, applying the automatically generated thresholds. Data normalization was performed with Scran (R v3.6.1), followed by log-transformation. Harmony was used for batch correction. Leiden clustering was applied with a resolution of 1. Marker genes for each cluster were computed and used, together with known canonical markers, to assign cell-type annotations. Velocyto was applied to estimate RNA velocity and PAGA was used to obtain an abstract graph representation of lineage connectivity between clusters. The scripts used for the analysis can be found under the following link; https://github.com/sgaedcke/sc_NK_AGLachmann .

Statistical analysis

Statistical analysis was performed using Prism version 9 (GraphPad). The type of analysis is indicated in the respective figure legends.

Materials availability

All stable reagents utilized/generated in this study could be provided upon request by the lead contact person and upon the completion of the necessary material transfer agreements. For further information and requests for the indicated reagents, all requests should be directed and will be fulfilled by Prof. Dr. Nico Lachmann (Lachmann.Nico@mh-hannover.de).

Data and code availability

scRNA sequencing datasets generated as part of this study are available at the NCBI (NCBI Accession: GSE273084).

Results

Planar and dynamic cultures support the continuous production and phenotype of iPSC-derived NK cells

Building on our previous work demonstrating the efficient production of iPSC-derived macrophages, granulocytes and myeloid progenitor cells [21, 30-32, 43, 44], we expanded this platform by guiding hematopoietic organoids toward NK cell differentiation. For this purpose, we employed a three-dimensional hematopoietic organoid system, referred to as hemanoids (Figure 1A). To initiate iNK cell production, hematopoietic organoids were generated according to the previously published protocol [30, 31]. To adapt the hematopoietic organoid system to iNK cell manufacturing, hematopoietic organoid generation was performed over a 10-day mesoderm priming phase, which entailed the following: On day 0, a single-cell solution of induced pluripotent stem cells was combined with mesoderm priming medium 1a (E8 medium supplemented with the mesoderm induction cytokines VEGF, BMP4, SCF, and Rock Inhibitor) at 70 rpm on an orbital shaker for 24 hours. On the following day, the medium was changed to mesoderm priming medium 1b (E6 media supplemented with VEGF, BMP4, SCF, and Rock Inhibitor) and the rotation speed was increased to 85 rpm. On days 4 and 7, medium was exchanged for the developing hematopoietic aggregates using mesoderm medium 2 (E6 medium supplemented with VEGF, BMP4, SCF, Rock Inhibitor, and IL3) (Figure S1A).

To facilitate the iNK lineage specification, we applied a cytokine combination previously described for NK cell differentiation (IL3, IL7, SCF, FLT3L, IL15) [35]. After completion of the 10-day mesoderm priming phase, the culture medium was replaced with NK differentiation medium (Xvivo15 supplemented with IL3, IL7, SCF, FLT3L, IL15, and Rock Inhibitor) (Figure 1A). The hematopoietic organoids were further cultured for multiple weeks, with the first cells appearing in the supernatant within several days following initiation of NK differentiation. After around four weeks (28 days), the first cell harvest was performed, and all subsequent cell harvests were performed on a biweekly rhythm (every 14 days). The cells shed from the organoids into suspension and were collected by simple medium exchange at weeks 4, 6, 8 and 10 yielding a total of 4 consecutive harvests (harvest 1-4, respectively).

To assess the robustness of the platform and its suitability for scalable culture formats, the differentiation process was performed in both adherent and suspension-based systems. Initial experiments were conducted at small scale using 6-well plates (3 mL culture volume per well), allowing quantitative assessment of cellular output. Hematopoietic organoids continuously produced iNK cells in both adherent and suspension-based cultures for up to 10 weeks (weeks 4, 6, 8 and 10), corresponding to harvest 1-4, respectively (Figure 1B). Cellular output varies depending on the culture method. In adherent cultures, the yields for harvests 1-

4 were 1.0 ± 0.4 x 10^6 cells/ well, 0.6 ± 0.2 x 10^6 cells/well, 0.3 ± 0.1 x 10^6 cells/well, 0.2 ± 0.04 x 10^6 (mean ± SD, n = 3-7), whereas in suspension cultures, the yields were 0.3 ± 0.1 x 10^6, 0.16 ± 0.08 x 10^6, 0.25 ± 0.06 x 10^6, 0.08 ± 0.03 x 10^6 (mean ± SD, n = 3-4). Overall, adherent cultures yielded approximately 3.1-, 3.7-, 1.3-, and 3.3-fold more iNK cells than suspension cultures across harvests 1-4, respectively (Figure 1B). Although adherent cultures yielded higher cell numbers, both systems demonstrated sustained and reproducible iNK cell production across multiple sequential harvests, indicating compatibility with both planar and suspension formats (Figure 1B). To quantify differentiation efficiency, total iNK cell output was normalized to the number of input iPSCs. Hematopoietic organoids generated 21.98 ± 5.6 iNK cells per input iPSC (mean ± SD, n = 7), corresponding to an approximately 22-fold increase, demonstrating efficient cellular amplification within this system (Figure 1C). Morphological assessment demonstrated that the hematopoietic organoids retained their overall structural integrity from the onset of NK cell production until the end of the culture period, when cell production had ceased (Figure S1B). In contrast, flow cytometric analysis revealed a significant reduction in the $CD34^+$ hematopoietic progenitor compartment between the beginning and end of NK cell production (Figure S1C), consistent with depletion of the progenitor population responsible for sustained NK cell production. This depletion of $CD34^+$ cells coincided with the cessation of iNK cell production, while the phenotypic characteristics of the generated iNK cells remained stable throughout the productive phase of the culture (Figure 1D), indicating that the decline in cellular output was associated with loss of hematopoietic progenitors rather than altered NK cell identity. Collectively, these findings establish that hematopoietic organoids enable continuous and scalable production of iPSC-derived NK cells across multiple weeks and culture configurations.

Phenotypic, transcriptional, and functional characterization of iPSC-Derived NK cell populations reveals progressive cell state from $CD56^-$ to $CD56^+$ states

Human NK cells are classically defined by the expression of CD45 and CD56, and the lack of expression of CD3 [45, 46]. To characterize iPSC-derived NK (iNK) populations, live $CD45^+/CD3^-$ cells were gated and analyzed based on CD56 expression, identifying $CD56^+$ and $CD56^-$ fractions across harvests 1-4 (Figure 1D; Figure S1D-E). Both adherent and suspension cultures, consistently generated $CD56^+$ iNK cells across all harvests. In adherent cultures, the ratio of $CD56^+$ cells was highest at harvest 1 and remained relatively stable thereafter ($CD56^+$: H1 86.54 ± 13.82%, H2 59.20 ± 28.27%, H3 66.13 ± 8.88%, H4 71.07 ± 26.95%, mean ± SD, n = 5) (Figure 1D; Figure S1E) and a similar trend was observed in suspension cultures ($CD56^+$: H1: 77.26 ± 9.49%, H2: 55.13 ± 22.16%, H3: 44.43 ± 7.81%, H4 44.30 ± 8.04%, mean ± SD, n = 3) (Figure 1D; Figure S1E), In both culture formats there was no significant difference in iNK cell ratios across all harvests in both adherent and suspension-based cultures (Figure S1E).

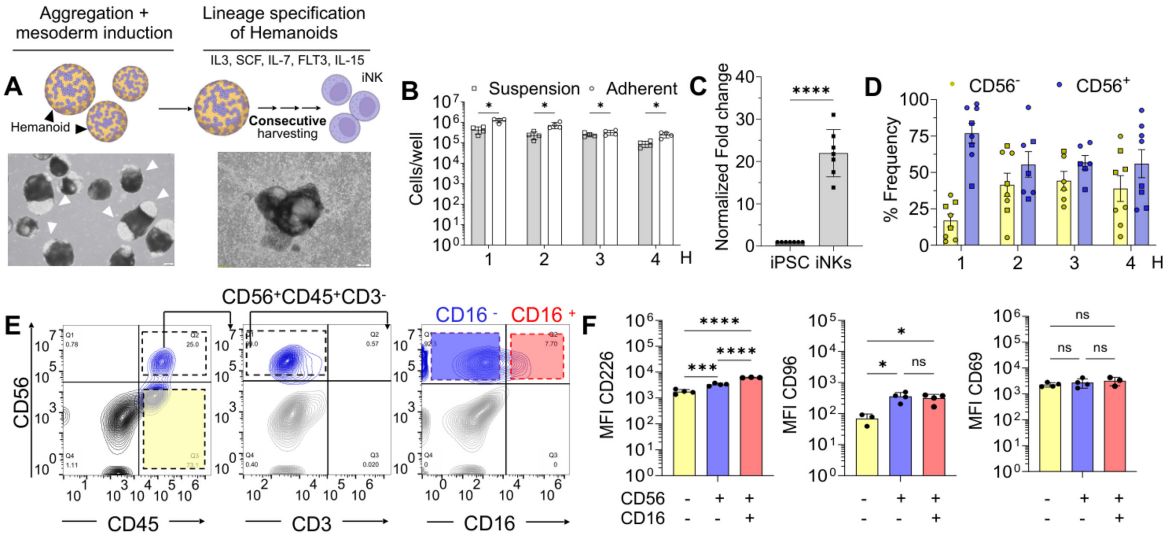


Figure 1. Continuous production of iPSC-derived Natural Killer cell (iNK) in planar and dynamic cultures. A Schematic representation of hiPSC hematopoietic organoid generation and differentiation towards Natural Killer cell lineage. **B** Cell production in adherent (circle) and suspension (square) -based small-scale (6 well) cultures across four sequential 4 harvests (means ± SD, n = 11), two-way ANOVA with Tukey's multiple comparisons test. **C** Conversion efficiency from iPSCs to iNK cells (means ± SD, n = 7), T-test. **D** Frequency of CD56% proportions in adherent (circle) and suspension (square) based cultures across all sequential harvests (means ± SD, n = 8). **E** Representative immunophenotypic plots of adherent based differentiation showing the major differentiation populations identified during iNK generation. **F** Expression of activating receptors CD226, CD96, and CD69 across iNK subsets (means ± SD, adherent: n = 2, suspension: n = 2, n = 4), one-way ANOVA with Tukey's multiple comparisons test.

Further resolution of the $CD45^+CD3^-$ compartment identified three principal iNK cell populations: $CD56^-CD16^-$ (yellow), $CD56^+CD16^-$ (violet), and $CD56^+CD16^+$ (red). Both adherent and suspension culture systems (adherent: Figure 1E; suspension: Figure S1F) generated phenotypically and morphologically comparable iNK cell subsets, indicating that differentiation format did not alter NK cell identity and morphology (Figure 1E; Figure S1D-G).

To further define iNK cell maturation states, activating and inhibitory receptor expression was evaluated across the three major subsets. $CD56^+CD16^+$ iNK cells exhibited significantly higher expression of the activating receptors DNAM-1 (CD226) and NKG2D compared with both $CD56^-CD16^-$ (yellow) and $CD56^+CD16^-$ (violet) populations (Figure 1F; Figure S1H, I). Similarly, inhibitory receptors TIGIT and NKG2A were significantly upregulated in $CD56^+CD16^+$ iNK cells (Figure S1H), whereas NKG2C expression did not differ among subsets (Figure S1H, I, J).

Additional receptor profiling of CD96 (an activation and adhesion marker), CD69 (an early activation marker), and CD94 (modulating receptor) revealed subset specific expression patterns across iNK cell populations. CD94 expression was highest in $CD56^-$ cells and significantly reduced in $CD56^+$ subsets (Figure S1H, J). In contrast, CD96 expression was significantly higher in $CD56^+$ iNK cells compared to $CD56^-$ cells (Figure 1F), consistent with increased activation and adhesion capacity. Despite this differential CD96 expression, CD69 levels were comparable across iNK cell subsets, indicating similar early activation states (Figure 1F). CD25 (IL-2Rα) was significantly elevated in $CD56^-$ cells compared to both iNK cell subsets (Figure S1H, J), suggesting cytokine responsiveness at earlier developmental stages. Thus, while CD96 was significantly enriched in $CD56^+$ fractions, this may suggest an increased potential for cell adhesion during activation. However, CD69 expression remained comparable across iNK cell subsets, indicating similar early activation states despite the differential expression of CD96. Analysis of killer immunoglobulin-like receptor (KIR) expression patterns (CD158a, CD158b1/b2j, CD158e) revealed minimal expression across subsets (Figure S2A, B), consistent with an early developmental phenotype lacking full NK cell education.

To further investigate the heterogeneity of $CD56^-CD16^-$, $CD56^+CD16^-$, and $CD56^+CD16^+$ populations, single-cell transcriptomic profiling was conducted. Uniform Manifold Approximation and Projection (UMAP) analysis revealed transcriptionally distinct clusters corresponding to phenotypically defined iNK cell populations, demonstrating heterogeneity within the differentiation systems (Figure S3A). Flow cytometric findings were corroborated at the transcriptional level, with enriched expression of canonical NK cell markers including *PTPRC*, *NCAM1*, *CD226*, *CD96*, and *CD69* within defined clusters (Figure 2A).

Gene signature scoring further supported a developmental hierarchy. Importantly, module scoring was performed as a complementary annotation approach and was not used to generate additional clusters. Instead, existing UMAP-defined populations were scored according to established NK cell developmental signatures to visualize the distribution of progenitor-like and mature NK cell states within the differentiation landscape. Cells lacking *NCAM1* expression showed higher enrichment of NK progenitor signatures, whereas $NCAM1^+$ populations were enriched for $NCAM1^+$ lymphocytes (Figure S4A), and mature NK cell signatures, enabling classification into NK progenitor like intermediates and mature NK cell states (Figure 2B, C; Figure S4A). Reference-based cell type prediction based on bone marrow reference datasets [47-50] confirmed hematopoietic origin of all cells, with predominant contributions from hematopoietic stem and progenitor cells and lymphoid populations, including NK cells, and smaller contribution from myeloid populations (Figure S4B, C).

Within the NK cell compartment, signature enrichment analyses performed across all identified iPSC-derived NK cell clusters revealed transcriptional similarity to previously described primary human NK cell states, including NK1, NK2, and NK intermediate populations (Figure 2C), consistent with established NK cell classification frameworks [51]. Previous transcriptomic analyses have demonstrated that NK1 and NK2 signatures represent distinct NK cell differentiation states, with NK1-like transcriptional programs associated predominantly with $CD56^{dim}$ NK cells, whereas NK2-like programs are associated with $CD56^{bright}$ NK cells. $CD56^{dim}$/NK1-like cells display features of more mature, cytotoxic NK cells, while $CD56^{bright}$/NK2-like cells represent a less terminally differentiated population characterized by enhanced cytokine production and developmental plasticity. Therefore, the presence of NK1- and NK2-like transcriptional programs across multiple iPSC-derived NK-cell clusters supports the generation of a heterogeneous NK cell compartment containing cells with different developmental and functional characteristics, rather than assigning individual clusters exclusively to a single NK cell subtype.

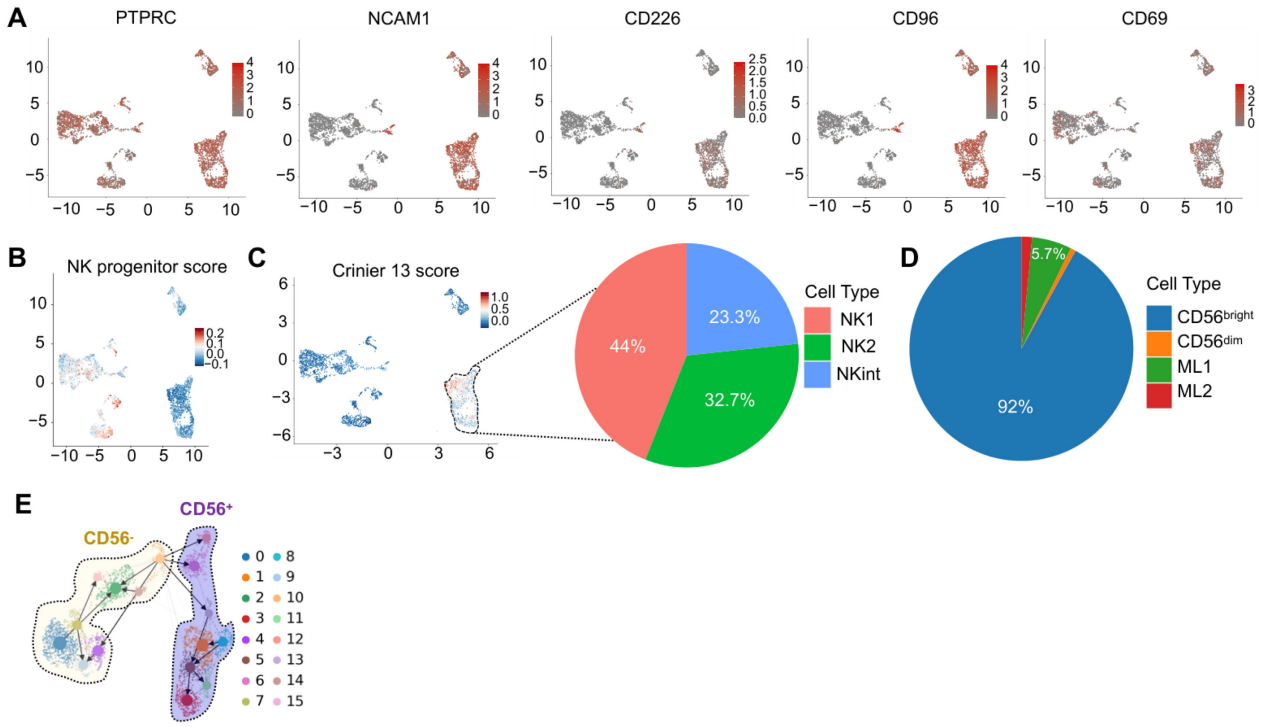


Figure 2. Transcriptomic analysis of iPSC-derived Natural Killer cells (iNK). A UMAP feature plots demonstrating global expression of *PTPRC* (CD45), *NCAM1* (CD56), *CD226* (DNAM-1), *CD96*, and *CD69*. **B** UMAP feature plot of NK progenitor score[40]. **C** UMAP feature plot of Crinier 13 gene score [40] demonstrating global expression (left) and the classification of the NK subsets (NK1, NK2, NKint) in pie chart (right). **D** Pie chart illustration NK functional subsets identified by Foltz et al [41] and annotated functional iNK subsets for memory-like (ML1 and ML2) or effector ($CD56^{bright}$ and $CD56^{dim}$) subsets. **E** PAGA trajectory analysis showing the transition from $CD56^{-}$ to $CD56^{+}$ populations.

To further characterize the transcriptional identity of the iPSC-derived NK cells, we performed an independent label transfer analysis using separate reference of primary human NK cells [41], which classifies NK cells into $CD56^{bright}$, $CD56^{dim}$, Memory-like (ML1), and Memory-like 2 (ML2) populations. This additional reference-based classification was included because Foltz et al. [41] demonstrated that cytokine stimulation with IL-12, IL-15, and IL-18 promotes the generation of cytokine induced memory-like NK cell populations, including ML1 and ML2 states, following NK cell activation and expansion. Although the cytokine-driven expansion phase is analyzed separately below, this reference framework was applied here to determine whether the iPSC-derived NK cell compartment contains transcriptional features corresponding to these established NK cell states prior to expansion. Label transfer analysis [41], also performed across the entire iPSC-derived NK cell compartment, further demonstrated functional correspondence with canonical NK subsets, including $CD56^{bright}$, memory-like 1 (ML1), memory-like 2 (ML2) cells, and $CD56^{dim}$, highlighting functional diversity within the NK compartment (Figure 2D; Figure S4D). Notably, $CD56^{bright}$ cells were predominant (Figure 2D), consistent with an early developmental state compared with peripheral blood NK populations, where $CD56^{dim}$ cells typically dominate [52].

To further track the transcriptional changes of cells with respect to *ZEB1* and *ZEB2*, given that *ZEB* family transcription factors regulate critical gene networks governing cell differentiation, maintenance, and functional specialization [53], we interrogated their expression dynamics across the identified *NCAM1* subsets. Feature plot analysis revealed distinct transcriptional differences between *NCAM1*$^{-}$ ($CD56^{-}$) and *NCAM1*$^{+}$ ($CD56^{+}$) populations, with $CD56^{-}$ cells preferentially expressing *ZEB2*, whereas $CD56^{+}$ cells showed higher expression of *ZEB1*, consistent with progressive NK cell differentiation (Figure S3A). Trajectory inference using partition-based graph abstraction (PAGA) revealed a continuum of transcriptional states connecting the identified clusters from *NCAM1*$^{-}$ ($CD56^{-}$) towards an *NCAM1*$^{+}$ ($CD56^{+}$), suggesting progressive transitions within the NK cell lineage (Figure 2E; Figure S3A).

To determine whether this transcriptional maturation corresponds to functional competence, cytotoxic activity and degranulation capacity were evaluated. iNK cells demonstrated significantly increased cytotoxic activity against K-562 target cells at a 5:1 effector to target ratio compared with 2:1, indicating functional dose responsiveness (Figure S4E) and demonstrated a significant lytic capacity compared to 2:1 and 5:1 ratios (Figure S4F). Consistent with this finding, CD107a mobilization was

significantly at both effector-to-target ratios, demonstrating that transcriptional maturation corresponded with acquisition of cytotoxic effector function (Figure S4E, F).

iNK expansion preferentially enriches cytotoxic iNK cell subsets, enhances effector function, and maintains transcriptional diversity

Building on our phenotypic and transcriptional characterization of iPSC-derived NK cells, we next investigated how *in vitro* expansion using artificial antigen presenting cells (aAPCs) expressing OX40L and membrane-bound IL18/IL21, in combination with soluble IL-2 and IL-15 [54, 55], influences iNK cell subset composition, effector function and transcriptional diversity (Figure 3A). Phenotypic profiling revealed extensive remodeling of the iNK cell compartment, characterized by a significant increase in $CD56^+$ iNK cells and a corresponding reduction in $CD56^-$ cells (Figure 3B). Prior to expansion, iNK distribution was $CD56^+CD16^-$: 55.23 ± 13.4%, $CD56^+CD16^+$: 2.11 ± 0.54%, $CD56^-CD16^-$: 35.66 ± 12.90% (mean ± SEM, n = 4). Following expansion, these proportions shifted to $CD56^+CD16^-$: 77.76 ± 4.5%, $CD56^+CD16^+$: 8.01 ± 5.44%, $CD56^-CD16^-$: 9.12 ± 1.85% (mean ± SEM, n = 4), indicating a preferential enrichment of $CD56^+$ iNK cell subsets (Figure 3B). Fold-expansion analysis demonstrated that $CD56^+CD16^+$ cells exhibited the highest proliferative capacity over the 14-day culture period (55.80 ± 26.11), followed by $CD56^+CD16^-$ cells (41.70 ± 28.35), whereas $CD56^-CD16^-$ cells expanded minimally (7.96 ± 3.5, mean ± SEM, n = 6) (Figure 3C).

Expanded iNK cells displayed robust upregulation of key activating receptors, including DNAM-1, KIRs, and CD69, across expanded $CD56^+$ NK populations (Figure 3D; Figure S4G-I), whereas inhibitory receptors such as CD94, NKG2A, and TIGIT showed either modest reduction or maintained expression levels (Figure 3D; Figure S4G-I). This receptor modulation suggests heightened responsiveness to stress ligands and enhanced effector function. Notably, $CD56^+$ NK cells retained expression of co-stimulatory and checkpoint receptors (CD94, NKG2A and TIGIT) following expansion, indicating maintenance of regulatory features despite proliferative stimulation (Figure 3D, E; Figure S4G-K).

To define transcriptional heterogeneity following expansion, single-cell transcriptomic sequencing was performed. UMAP analysis revealed closely related but molecularly distinct NK cell clusters, indicating preservation of subset diversity (Figure 3F; Figure S5A). Cell-cycle analysis showed predominant expressions of G1 and G2/M phase gene signatures, with a smaller fraction in S phase (Figure S5B). Four major transcriptional clusters (0, 1, 2, and proliferating) were identified by molecular features[51]. Cluster 0 expressed *NCAM1*, *FCGR3A*, *ITGAM*, and *ITGAX*; Cluster 1 expressed *NCAM1* and *ITGAX* but lacked *FCGR3A* and *ITGAM*; Cluster 2 expressed *FCGR3A* alone; whereas the proliferating cluster lacked all four markers (Figure 3G). Consistent with these transcriptional profiles, the clusters aligned with distinct immunophenotypic subsets identified by flow cytometry, with Cluster 0 corresponding to $CD56^+CD16^+$, Cluster 1 to $CD56^+CD16^-$, and Cluster2 and proliferating population corresponding predominantly to $CD45^+CD56^-$ fraction (Figure 1E; 3F, G; Figure S1F, 5A).

Each cluster displayed distinct cytokine and effector transcriptional programs. The Proliferating cluster revealed minimal expression of activation markers and maturation-associated genes including *CXCR3*, *KLRK1*, *IL12RB2*, *IL15RA*, and *GSDMD*. Cluster 2 demonstrated robust transcription of cytokines including *IFNG*, *XCL2*, *IL32*, *XCL1*, *CCL5*, *CSF1*, *CCL3*, *CSF2*, *CCL4*, *CCL4L2*, *IL16*, and *FLT3LG*, whereas Cluster 1 expressed *IFNG*, *TNF*, *XCL1*, *XCL2*, and *IL32*, and Cluster 0 preferentially expressed *CCL5*, *CSF1*, *CCL3* (Figure 3G).

At the protein level, the corresponding $CD56^+$ subsets had higher expression of NKG2C, NKG2A, DNAM-1, KIRs, and TIGIT compared with $CD56^-$ cells, consistent with transcriptomic finding (Figure 3E; Figure S4J, K). Cell-type annotation using human hematopoietic reference datasets [47-50] confirmed 98% NK cell purity following expansion (Figure 3H; Figure S5C, D). Subset classification revealed predominance of NK2 (68.2%), followed by NK1 (30.9%), and a minor NK intermediate population (0.9%) (Figure S5D, E). Functional identity prediction using label transfer [41] demonstrated enrichment of $CD56^{bright}$, ML1, ML2, and $CD56^{dim}$, in descending order of abundance (Figure 3I; Figure S5F).

Expanded populations were enriched for transcripts encoding cytotoxic effector molecules and activation-associated pathways, including *IFNa*, *IFNG*, *mTORC1* signaling components (Figure S5G), *GZMA*, *PRF1*, *TNFSF10*, *GSDMB*, *KLRC2* (NKG2C), and *KLRK1* (NKG2D) (Figure 3G). In contrast, inhibitory receptors *KLRC1* (NKG2A) expression was highest within Cluster 0 ($CD56^+CD16^+$) cells, reflecting their regulatory phenotype (Figure 3G; Figure S4J, K). Together, the concordance between the transcriptionally defined clusters, their corresponding flow cytometric phenotypes and functional properties suggest that expansion preserves distinct iNK cell subsets while selectively enriching cytotoxic populations.

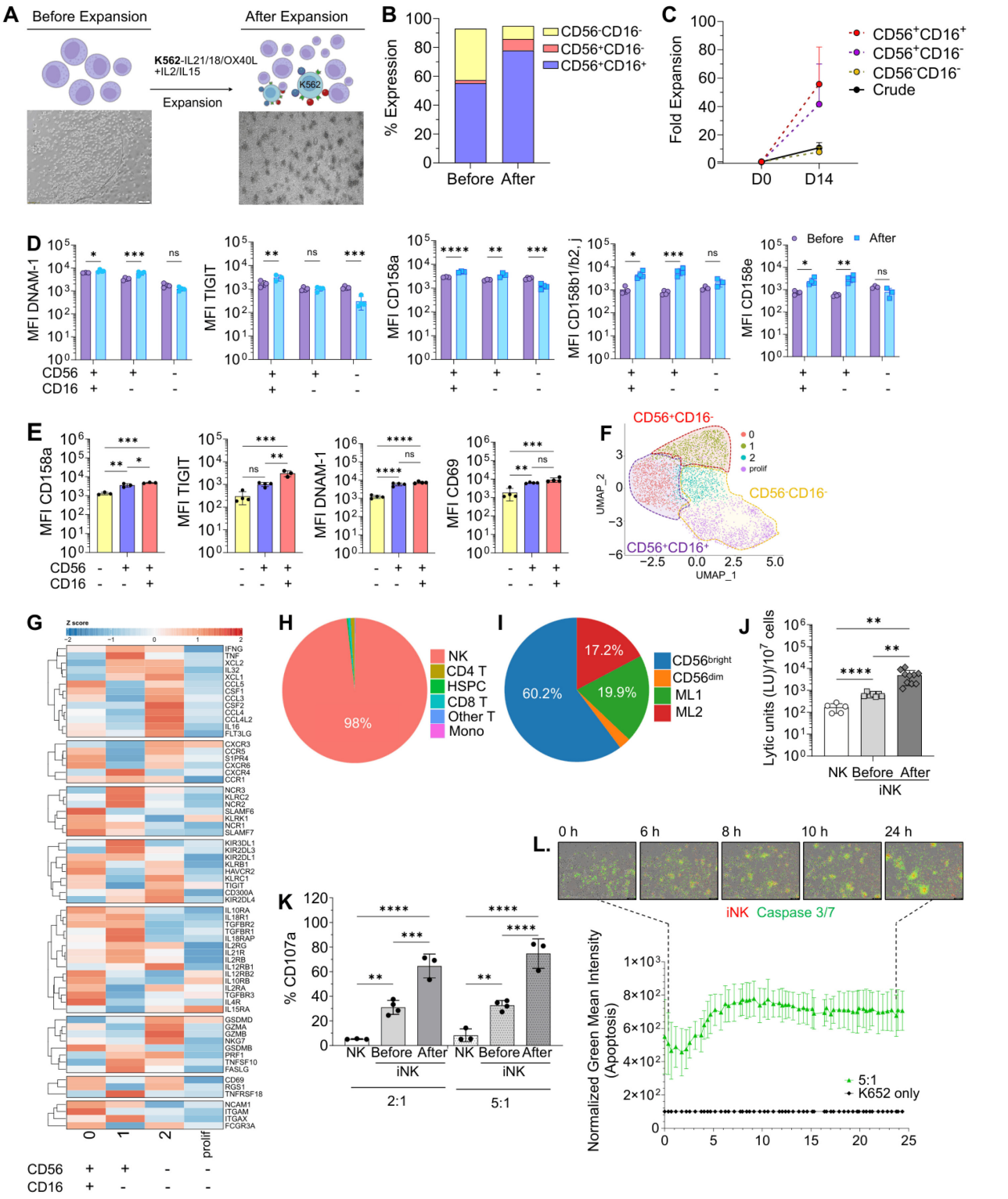


Figure 3. NK expansion preferentially enriches cytotoxic NK subsets, enhances effector function, and maintains transcriptional diversity. A Schematic overview of iNK cells collected from sequential differentiation harvests and subsequently expanded using K562-IL21/18/OX40L + IL2/15 (aAPCs). **B** Distribution of iNK subsets profile before and after expansion (n = 4). **C** Fold expansion of iNK subsets (means ± SEM, n = 6). **D** Expression of activating receptor, inhibitory receptor, and KIRs across iNK subsets before and after expansion (means ± SD, adherent: n = 2, suspension: n = 2, n = 4), two-way ANOVA with Šídák's multiple comparisons test. **E** Expression of selected receptors (CD158a, TIGIT, DNAM-1, and CD69) across expanded iNK subsets (means ± SD, adherent: n = 2, suspension: n = 2, n = 4), one-way ANOVA with Tukey's multiple comparisons test. **F** UMAP visualization of expanded iNK subsets (CD56^{+}CD16^{+}: red, CD56^{+}CD16^{-}: violet, CD56^{-}CD16^{-}: yellow). **G** Heatmap depicting differential expression of selected marker genes associated with cytokines signaling, chemotaxis, activation, inhibition, and cytotoxic molecules across iNK cell subsets. Expression values are z-score normalized, with the color gradient ranging from −2 (blue) to 2 (red). **H** Pie chart illustration of cell types after expansion. **I** Pie chart illustration of functional iNK subsets after expansion for memory-like (ML1 and ML2) or effector (CD56^{bright} and CD56^{dim}) subsets identified by Foltz et al [41]. **J** Cytotoxic activity in lytic units against K562 target cells of *ex vivo* NK cells and iNK cells before and after expansion (means ± SD, n = 5-7), one-way ANOVA with Dunnett's multiple comparisons test. **K** Cytotoxic activation against K562 in CD107a activity of *ex vivo* NKs and iNK cells before and after expansion (means ± SD, adherent: n = 2, suspension: n = 2, n = 4), one-way ANOVA with Šídák's multiple comparisons test. **L** Representative fluorescence images of iNK cells (red) and K-562 co-culture over 24hours, together with quantification of Caspase-3/7 activity (green) over time (mean ± SD, n = 3).

To determine whether these transcriptional reprogramming corresponded to functional competence following expansion, iNK cells exhibited significantly enhanced cytotoxic effector activity against K-562 target cells, with increased lytic function at both 2:1 effector-to-target ratios (31.01 ± 2.09% pre-expansion vs 58. ± 1.95% after expansion; mean ± SEM, n = 3-6) and 5:1 ratios (47.97 ± 5.07% vs 66.74 ± 1.49%; mean ± SEM, n = 3-6) and significantly increased lytic killing after expansion and before expansion in comparison to *ex vivo* NK cells (Figure 3J; Figure S5G). Similarly, cytotoxic activation followed the same trend, with both pre- and post-expansion iNK cells exhibiting significantly greater degranulation capacity than *ex vivo* NK cell controls, indicating that expansion further enhanced an already elevated functional response (Figure 3K). Live-cell imaging confirmed sustained induction of target cell apoptosis over 24 hours (Figure 3L), which was accompanied by robust secretion of cytolytic effector molecules, including interferon-γ (IFN-γ), perforin, granzyme A, granzyme B, and granulysin, consistent with an active cytotoxic response (Figure S5H, I, J). Furthermore, assessment of migratory behavior in an HCMV-infected human lung tissue model demonstrated that iNK cells exhibited migration characteristics comparable to donor-derived peripheral blood NK cells (pNK), with no significant differences in track speed, acceleration, track straightness, or displacement length, indicating preserved trafficking capacity following differentiation (Figure S5K). Differential pathway enrichment analysis of top 5 differentially expressed genes (DEGs) across clusters revealed significant activation of Interferon responses and mTORC1 signaling pathways, consistent with enhanced effector programming (Figure S5H).

Collectively, these findings demonstrate that *in vitro* expansion preferentially promotes the proliferation of cytotoxic iNK cell subsets, upregulates key activating and effector molecules, enhances cytotoxic function, degranulation, and secretion of cytolytic effector mediators, while preserving migratory capacity, subset heterogeneity, transcriptional complexity, and functional activity.

Up-scaling the generation of iPSC-NK cells in a benchtop bioreactor

To assess the scalability and phenotypic stability of iNK cell generation, we generated hematopoietic organoids in a 50 mL benchtop bioreactor (Figure 4A) and compared them to small-scale cultures. Bioreactor cultures supported robust and sustained cell production across three consecutive harvests, yielding $4.3 \times 10^7 \pm 2.9 \times 10^7$, $1.1 \times 10^7 \pm 0.5 \times 10^7$, and $0.4 \times 10^7 \pm 0.9 \times 10^6$, mean ± SEM, n = 4), respectively, corresponding to a cumulative yield of 5.7×10^7 cells, which was higher than that obtained from small-scale differentiation (Figure 4B, 1B). When normalized to culture volume, however, cell production per milliliter was comparable between the small- and moderate-scale systems, with no significant differences observed, indicating that the increased total cell yield in the bioreactor was attributable to the larger culture volume rather than enhanced volumetric productivity (Figure S6A). Despite this increased cumulative yield, in contrast to the small-scale (3 mL) cultures, which remained productive across four sequential harvests, iNK cell output in the 50 mL bioreactor declined earlier, with productive release from the aggregates ceasing after the third harvest. Consequently, only three harvests were obtained under medium-scale conditions, indicating a reduced duration of productive output despite the higher cumulative yield. To quantify differentiation efficiency, total iNK cell output was normalized to the number of input iPSCs. Hematopoietic organoids generated 48.62 ± 39.92 iNKs per input iPSC (mean ± SD, n = 4), corresponding to an approximately 50-fold increase, demonstrating efficient cellular amplification within this system (Figure 4C).

Phenotypic analysis revealed comparable distribution of $CD56^+$ and $CD56^-$ populations across sequential harvests, with enrichment of $CD56^+$ iNK cells in the first harvest followed by gradual reduction over time ($CD56^+$: H1 77.6 ± 21.9%, H2 67.5 ± 32.6%, H3 42.0 ± 7.5%, mean ± SD, n = 4) (Figure 4D). These trends mirrored those observed in six-well plate cultures (Figure S6B), indicating that bioreactor-based production preserves iNK cell developmental kinetics during long term culture.

To further define bioreactor-derived iNK cell receptors, we performed expression profiling of natural cytotoxicity receptors (NCRs), including NKp46, NKp44, NKp30. The majority of $CD56^+$ cells generated in the bioreactor were phenotypically mature for NKp46 (98.72 ± 1.0%, mean ± SD, n = 6), NKp44 (61.24 ± 12.2%, mean ± SD, n = 6), and NKp30 (74.7 ± 21.3%, mean ± SD, n = 6). In contrast, $CD56^-$ cells exhibited substantially lower expression of NKp46 (50.0 ± 28.6%, mean ± SD, n = 6), NKp44 (3.07 ± 2.8%, mean ± SD, n = 6), and NKp30 (2.6 ± 3.0%, mean ± SD, n = 6) (Figure 4E), consistent with early NK precursor phenotype. Further resolution of the bioreactor-derived iNK cells identified three subsets, $CD45^+CD3^-$ expressing $CD56^-CD16^-$ (yellow), $CD56^+CD16^-$ (violet), and $CD56^+CD16^+$(red), consistent with small-scale cultures (Figure 4F; 1E; Figure S1F, 6C), mirroring the morphological and phenotypic distribution observed in small-scale cultures. Consistent with these corresponding subsets,

$CD56^+$ populations exhibited higher expression of activating receptors, inhibitory receptors, and KIRs than the $CD56^-$ fraction, demonstrating preservation of the receptor landscape across culture scale (Figure 4G; Figure S6D-G).

To further characterize the functional competence and checkpoint balance of bioreactor-derived iNK cell subsets following scale-up, we performed comprehensive phenotypic and activation profiling of the various iNK cell populations. Functional and phenotypic analysis demonstrated significant upregulation of activation receptors DNAM-1, CD96, CD69, and NKG2D in $CD56^+$ iNK populations relative to $CD56^-$ populations (Figure 4G; Figure S6D). Inhibitory receptors TIGIT and NKG2A were also elevated in $CD56^+$ populations (Figure 4G; S6D), suggesting intact checkpoint regulation. These profiles were comparable to those observed in 6-well plate cultures, confirming that up-scaling to the benchtop bioreactor does not compromise effector features (Figure S6E).

To assess the effect of *in vitro* expansion of bioreactor-derived iNK cell, we performed comprehensive phenotypic, and functional analysis before and after expansion. Following expansion with aAPCs, bioreactor-derived iNK cells exhibited extensive remodeling of the iNK cell compartment, characterized by a marked increase in $CD56^+$ iNK cells and a concomitant reduction in $CD56^-$ cells. Prior to expansion, iNK subsets distribution was $CD56^+CD16^-$: 20.30 ± 3.4%, $CD56^+CD16^+$: 39.34 ± 13.1%, $CD56^-CD16^-$: 38.3 ± 11.9% (mean ± SEM, n = 6). After expansion, proportions shifted to $CD56^+CD16^-$: 26.0 ± 5.9%, $CD56^+CD16^+$: 57.1 ± 9.8%, $CD56^-CD16^-$: 16.8 ± 4.2% (mean ± SEM, n = 6), indicating a preferential outgrowth of more mature iNK subsets, consistent with small-scale observations (Figure 4H, 3B). Notably, expanded iNK cells also displayed robust downregulation of key inhibitory receptors, including TIGIT and NKG2A, together with upregulation of KIRs and CD69 across expanded $CD56^+$ iNK cell populations, further indicating phenotypic maturation and enhanced activation following expansion (Figure 4I; S6G; S7A).

To further characterize the functional consequences of expansion across different production scales, we evaluated both degranulation capacity and cytolytic effector molecule secretion in small-scale and bioreactor-derived iNK cells compared with expanded primary NK cells. Degranulation analysis demonstrated that expanded iNK cells regardless of scale exhibited significantly higher CD107a mobilization compared with expanded *ex vivo* NK cells, indicating enhanced cytotoxic responsiveness following expansion (Figure S7B). The CD107a degranulation response of expanded *ex vivo* NK cells ranged from approximately 5-20%, which may reflect the donor- and assay-dependent variability commonly observed in NK cell degranulation responses. Despite this increased degranulation capacity, expanded iNKs secreted comparable levels of cytolytic effector molecules, including interferon-γ (IFN-γ), granzyme A, granzyme B, perforin, and granulysin, relative to expanded primary NK cells, demonstrating that scalable manufacturing preserves the functional secretory profile of iNK cells (Figure S7C, D). Together, the enhanced degranulation observed in expanded iNK cells and the comparable secretion of IFN-γ, perforin, granzymes, and granulysin, suggest that expansion primarily increased the frequency of cytotoxic responses rather than altering the amount of effector molecules released per responding cell. A similar pattern was observed during K-562 target cell apoptosis, where both small-scale and bioreactor-derived iNK cells secreted comparable amounts of IFN-γ, granzyme A, granzyme B, perforin, and granulysin following co-culture, further demonstrating that iNK cells retain a consistent cytolytic secretory profile irrespective of the production scale (Figure S7E, F).

Receptor profiling revealed significant decrease in inhibitory receptors including TIGIT, CD94, NKG2A (Figure 4J, K; Figure S6G). Although overall KIR expression prior to expansion is low however, after expansion KIR expression in $CD56^{+/-}$ subsets displayed significantly higher KIR expression compared to before expansion populations (Figure 4K, L; Figure S6E). These coordinated phenotypic changes indicate activation associated receptor remodeling during expansion in the bioreactor system, consistent with small-scale cultures (Figure S6E).

Importantly, no significant differences were detected between bioreactor-derived and plate-derived iNK cells with respect to morphology, cellular output, iNK cell populations, receptor profile expression, checkpoint marker distribution, KIR levels, or cytotoxic protein expression, demonstrating phenotypic concordance across manufacturing formats. Functional capacity was similarly preserved, confirming that scale-up did not impair effector potential (Figure S6; Figure S7).

Collectively, these findings demonstrate that up-scaling iNK cell production in a 50 mL benchtop bioreactor enables sustained, reproducible, and phenotypically stable generation of functional iNK cells. This scalable bioprocess preserves subset composition, receptor expression, and effector function, underscoring its suitability for translational iNK cell manufacturing.

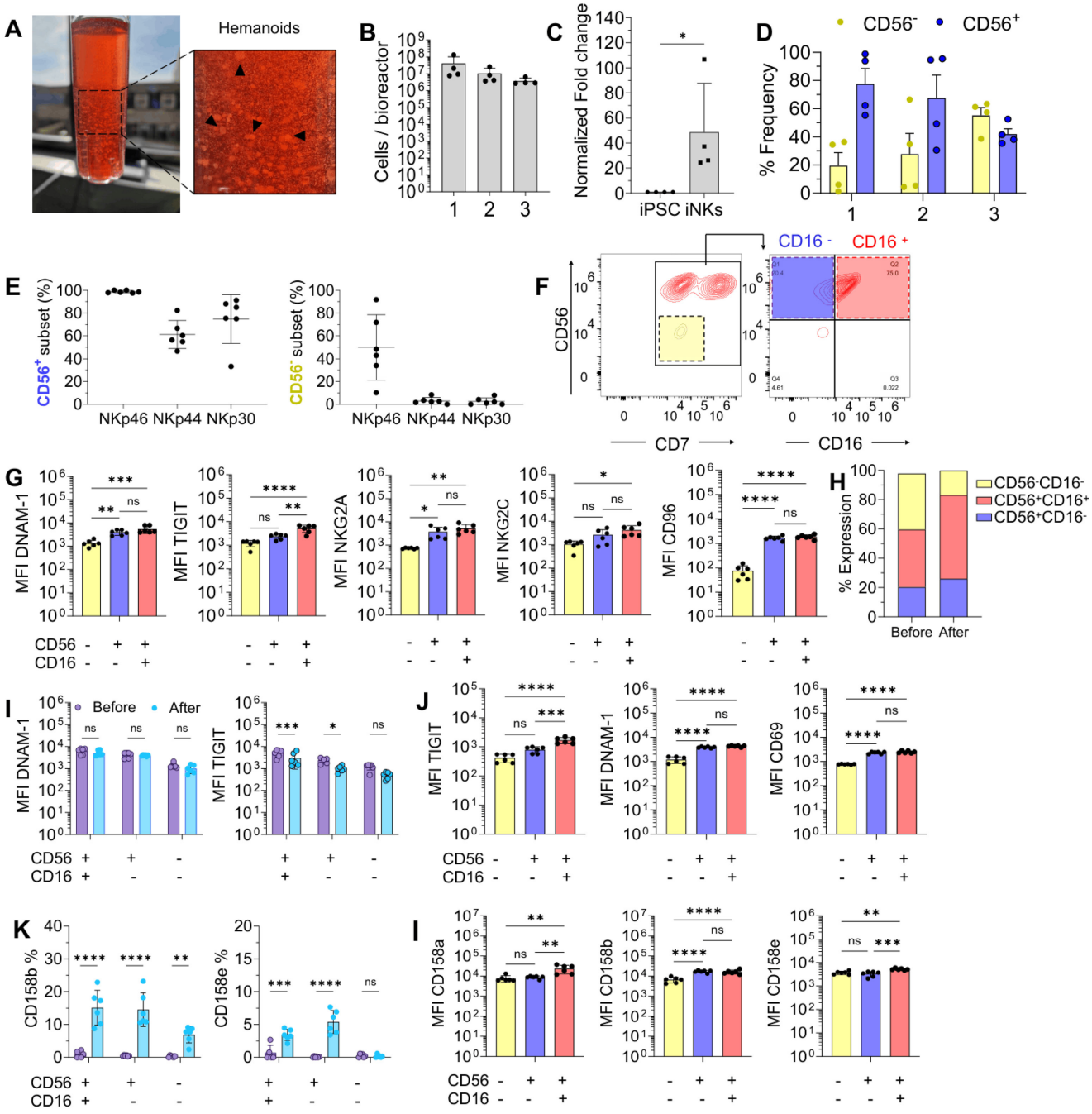


Figure 4. Up-scaling the manufacturing of continuous production of iPSC-NK cells in a benchtop bioreactor. A Representative image of iNK cell differentiation within a 50 mL bioreactor tube. Arrows indicate the hemanoid activity releasing iNK cells into the culture medium (scale bar 200 µm). **B** Cell production from bioreactor cultures across 3 sequential harvests (mean ± SD, n = 4). **C** Fold expansion of iNK subsets (means ± SEM, n = 4), T-test. **D** CD56% proportions across all sequential harvests (1, 2, and 3) (mean ± SD, n = 4). **E** Natural cytotoxicity receptor profile (NCR) assessment of NKp46, NKp44, and NKp30 $CD56^+$ (left) and $CD56^-$ (right) fractions (mean ± SD, n = 7). **F** Representative immunophenotypic plots of bioreactor-based differentiation of iNK subsets. **G** Expression of activating and inhibitory receptors across bioreactor-derived iNK subsets prior to expansion (mean ± SD, n = 6), one-way ANOVA with Tukey test. **H** Distribution of bioreactor-derived iNK subsets before and after expansion (mean ± SD, n = 4). **I** Expression of CD226 and TIGIT across bioreactor-derived iNK subsets before and after expansion (mean ± SD, n = 6), Two-way ANOVA with Šídák's multiple comparisons test. **J** Expression of activation and inhibitory receptors in expanded bioreactor-derived iNK subsets after expansion (mean ± SD, n = 6), one-way ANOVA with Tukey's multiple comparisons test. **K** Expression levels of KIRs across bioreactor-derived iNK subsets before and after expansion (mean ± SD, n = 6), two-way ANOVA with Šídák's multiple comparisons test. **L** Expression levels of KIRs across bioreactor-derived iNK subsets after expansion (mean ± SD, n = 6), one-way ANOVA with Tukey's multiple comparisons test.

Discussion

The capacity to generate functional natural killer (NK) cells from human induced pluripotent stem cells (iPSCs) at scale remains a critical challenge for the advancement of universal, "off-the-shelf" cell-based immunotherapies. Here, we establish a continuous and scalable platform for the generation of iPSC-derived NK (iNK) cells using hematopoietic organoid cultures ("hemanoids") that enables serial harvests

over extended periods and can be readily transferred to standardized bioreactor systems without loss of cellular function or phenotypic stability. This platform addresses persistent bottlenecks in iNK cell manufacturing yield, scalability, and reproducibility, while preserving transcriptional and functional diversity characteristics of iPSC-derived NK cell biology.

Unlike conventional feeder-based or embryoid body protocols that typically produce a single harvest [26, 56], our hematopoietic organoid system supports continuous iNK cell production for up to ten weeks with multiple harvests. The ability to repeatedly collect $CD45^+CD7^+CD56^{+/-}$ NK cells from the same culture expands output by over an order of magnitude compared to batch protocols, substantially improving the iPSC-to-NK conversion ratio (1:22). The long-term shedding of mature NK cells suggests that organoid microenvironments provide a self-renewing hematopoietic niche capable of maintaining progenitor activity and lineage commitment over time, an emergent feature absent in monolayer or embryoid body differentiation systems.

Flow cytometric and single-cell transcriptomic profiling revealed canonical NK cell differentiation trajectories delineated a continuum from precursor/progenitor ($CD56^-$) to iNK cell ($CD56^+$) phenotypes, indicating that our platform recapitulates key aspects of early human NK development. The emergence of transcriptionally distinct iNK subsets classified as NK1, NK2, and NK intermediate, displayed phenotypic and transcriptional characteristics consistent with functionally diverse NK cell states. Their gene-expression profiles showed qualitative overlap with previously described NK transcriptional programs [41, 51]. Furthermore, we did not identify a transcriptionally distinct NK3-like population in our dataset. This may reflect differences between *in vitro* differentiation and *in vivo* NK maturation, where NK3 populations have been associated with late-stage maturation states that may require additional environmental cues not present in the current differentiation system. Together, these observations suggest that iPSC-derived NK cells capture elements of NK developmental diversity while not fully recapitulating the complete spectrum of peripheral NK subset heterogeneity. The presence of activation-associated transcriptional signatures, including features associated with cytokine-induced memory-like (CIML) profiles, therefore further underscores the developmental plasticity preserved in this system, echoing recent single-cell analyses of human NK diversity [41, 51].

Expansion with aAPCs expressing OX40L and membrane-bound IL-18/IL-21 selectively enriched for cytotoxic $CD56^+$ NK cells, concomitant with increased expression of activating receptors (DNAM-1, NKG2D) and effector molecules (*GZMA*, *PRF1*, *TNFSF10*), reflecting enhanced functional maturation. These transcriptional changes translated into enhanced functional competence, as expanded iNK cells displayed increased cytotoxicity, sustained target-cell apoptosis, and significantly greater CD107a degranulation than expanded primary NK cells. Interestingly, despite their enhanced degranulation, expanded iNK cells secreted comparable amounts of IFN-γ, perforin, granzyme A, granzyme B, and granulysin, suggesting that expansion primarily increased the proportion of functionally responsive cytotoxic cells rather than the amount of effector molecules released per responding cell. These findings are in line with prior reports that IL-18/IL-21 signaling promotes NK cytotoxic maturation and metabolic reprogramming [41]. While expansion effectively increased $CD56^+$ populations and cytotoxic competence, the overall expansion fold achieved for iPSC-derived NK cells (~48.5-fold) remains substantially lower than what is routinely observed for primary NK cells, which can exceed 1000-fold under optimized expansion conditions. This limitation is consistent with previous reports of iPSC-derived NK cell expansion [57, 58] and highlights an intrinsic difference in proliferative capacity between iPSC-derived and peripheral blood NK cells. These findings indicate that while iPSC-derived NK cells can acquire enhanced functionality through *ex vivo* expansion, additional strategies including optimized cytokine combinations, co-stimulatory signaling, or genetic modifications, may be required to achieve expansion levels comparable to primary NK counterparts.

Moreover, parallels between our expanded iNK cells and cytokine-induced memory-like (CIML) NK cells are notable. CIML NK cells, generated by short-term stimulation with IL-12, IL-15, and IL-18, exhibit hallmark features such as heightened IFN-γ responsiveness, increased cytotoxicity, metabolic priming, and improved persistence driven by stable transcriptional and epigenetic remodeling [41, 59-63]. Our expanded iNK cells similarly demonstrate robust cytotoxic function, elevated activating-receptor expression, and activation-associated transcriptional programs that align with CIML NK phenotypes, together with enhanced degranulation and sustained induction of target-cell apoptosis. The preservation of cytolytic effector molecule secretion despite increased degranulation further suggests that expansion preferentially enhances cytotoxic responsiveness while maintaining a stable secretory phenotype, suggesting that the expansion environment promotes a memory-like functional state. Importantly, beyond

their cytotoxic competence, iNK cells also exhibited migratory behavior comparable to donor-derived peripheral blood NK cells in an HCMV-infected human lung tissue model. Similar track speed, acceleration, displacement, and directional persistence suggest that the differentiation process preserves key migratory properties associated with NK cell tissue surveillance and target-cell engagement. Although classical CIML NK cells acquire durable epigenetic imprinting and enhanced recall responses that may not yet be fully recapitulated in our system, the close functional alignment between expanded iNK cells and CIML NK cells indicates that iPSC-derived populations can inherently adopt CIML-like features. These findings highlight a strong foundation upon which targeted cytokine priming or memory-inducing cues could further consolidate CIML characteristics within iNK cell manufacturing workflows.

Notably, in contrast to primary NK cells, our expanded iNK cells retained high levels of inhibitory checkpoint receptors (TIGIT, NKG2A). Furthermore, NKG2A expression was higher in $CD56^{+}CD16^{+}$ compared with $CD56^{+}CD16^{-}$ cells, which is opposite of what is typically observed in primary NK cells [64], This pattern suggests that iPSC-derived hematopoiesis may follow an embryonic or fetal-like developmental trajectory, characterized by distinct inhibitory receptor dynamics [65], which may help preserve regulatory control, an advantageous feature for safety in therapeutic applications. The observed activation of *IFNG* and *mTORC1* pathways mirrors transcriptional programs associated with effector NK cell activation [66-68].

Importantly, these regulatory features gain additional significance in light of emerging evidence that NK cells are not merely bystanders but direct drivers of late-stage antibody-mediated rejection in solid organ transplantation. In allogeneic settings, mismatches in MHC class I molecules can disrupt inhibitory signaling through receptors such as KIRs and NKG2A, triggering NK cell activation via "missing-self" recognition. Activated NK cells can further contribute to graft injury through CD16-mediated antibody-dependent cellular cytotoxicity (ADCC), particularly in sensitized recipients with pre-existing donor-specific antibodies. Infiltrating $CD16^{+}$ NK cells have been robustly associated with microvascular inflammation, endothelial damage, and graft dysfunction, while CD38-expressing NK subsets have emerged as key pathogenic mediators and therapeutic targets. The retention of inhibitory receptor expression in iPSC-derived NK cells may therefore provide an intrinsic safety buffer, potentially limit unchecked cytotoxicity while preserve responsiveness to activating cues. Although our iNK cells expressed CD16 and exhibited robust cytotoxic function, ADCC was not directly assessed in this study. Future work should therefore include comparative ADCC analysis with *ex vivo* and expanded primary NKs, particularly in the context of therapeutic anti body-based applications. These observations reinforce the importance of controlling NK cell maturation state and subset composition when developing broadly applicable iNK cell therapies.

In parallel with these maturation-related considerations, donor immunogenetics represent an important upstream variable for iPSC-based NK cell manufacturing. The review by Biederstädt et al. [69] underscores that polymorphisms in KIR gene content, HLA ligand background, and FcγR variants can influence NK licensing, cytotoxic potential, and response to antibody-dependent strategies. Although iPSC differentiation may attenuate or reset components of *in vivo* education, strategic donor selection at the iPSC-derivation stage could nevertheless optimize foundational receptor repertoires and enhance downstream functional capacity. These insights suggest that donor selection frameworks developed for primary NK cell therapy may require adaptation for iNK cell systems but remain highly relevant as part of an integrated approach to achieving mature, clinically potent NK cell phenotypes.

Up-scaling to a 50 mL benchtop bioreactor achieved $>5.7 \times 10^{7}$ iNK cells prior to expansion, while increasing differentiation efficiency to approximately 49 iNK cells per input iPSC (~50-fold amplification), maintaining iNK cell subset composition, receptor expression, and cytotoxic function, confirming that hemanoid-based differentiation is compatible with dynamic culture and scalable manufacturing. A recent first-in-human trial [70] demonstrated tolerability iNK cell doses reaching 1.8×10^{9} cells per cycle. Our platform generates 5.6×10^{7} iNK cells pre-expansion, which combined with an average 48.5-fold expansion, produces approximately 2.7×10^{9} cells, sufficient for a single treatment cycle and potentially scalable for multi-patient production using larger bioreactors. Comparable receptor and effector profiles between small-scale and bioreactor-derived NK cells indicate that mechanical and shear forces at this scale do not perturb developmental trajectories or maturation kinetics, in contrast to previous reports of impaired cytotoxic activity or altered subset ratios during stirred-suspension culture [71]. Furthermore, bioreactor-derived iNK cells retained phenotypic composition, cytotoxic activity, degranulation capacity, and cytolytic effector molecule secretion comparable to small-scale cultures following expansion, demonstrating that increased

manufacturing scale does not compromise functional potency. Reproducibility across platforms supports translational feasibility for scalable GMP-compliant manufacturing, where bioreactor integration and continuous harvest could substantially reduce cost per therapeutic dose. In addition, transitioning from labor-intensive planar culture systems to closed or semi-closed bioreactor-based workflows may reduce operator intervention, facility utilization, and batch-to-batch variability. The combination of continuous NK cell bioreactor production and expansion therefore has the potential to improve overall manufacturing economics relative to conventional single-harvest differentiation protocols. Moreover, the expansion strategy described here employs comparatively low cytokine concentrations (20 IU/mL IL-2 during the first week followed by 100 IU/mL IL-2 and 10 ng/mL IL-15 during the second week), substantially lower than the 500 IU/mL IL-2 commonly used in conventional NK cell expansion protocols. Reduced cytokine requirements may therefore further decrease manufacturing costs while maintaining efficient expansion and functional maturation. Nevertheless, future studies incorporating formal cost-of-goods modeling will be required to quantify the economic benefits of this approach and identify the major remaining cost drivers within the manufacturing process.

Despite these advances, several challenges remain. Our iNK cells exhibit low KIR expression across subsets, indicating an immature phenotype consistent with incomplete "education," as previously reported in iPSC-derived NKs [26, 72]. This may limit *in vivo* persistence and self-tolerance, suggesting that additional licensing cues such as HLA engagement or cytokine modulation, could be required for full maturation. Importantly, KIR expression in our iNK cells was predominantly observed after expansion and therefore differs from the primary NK cells. In particular, $CD56^{bright}$ iNK cells expressed KIRs after expansion, which is opposing to their primary counter parts [26, 52, 73]. This phenotype, however, is in concordance with other reports of iPSC-derived NK cells [26, 72], and warrants further investigation, particularly in light of evidence from murine models indicating that $CD56^{bright}$ and $CD56^{dim}$ NK cells emerge from separate progenitor lineages rather than a shared linear developmental trajectory [74], as $CD56^{bright}$ and $CD56^{dim}$ do not exist in mice, in contrast to NK2 and NK1 which are conserved across species. Nevertheless, our current workflow involves two distinct stages, differentiation followed by expansion, which introduces additional complexity and processing time. Developing a unified, single-step protocol that integrates both differentiation and expansion would streamline production and improve scalability for clinical translation.

Notably, emerging evidence suggests that the immature nature of iPSC-derived NK cell populations may not necessarily represent a disadvantage for therapeutic applications. Recently, Wang et al. demonstrated that pluripotent stem cell-derived induced NK progenitor (iNKP) cells exhibit robust *in vivo* engraftment, prolonged persistence, and continuous generation of functional NK cells, resulting in sustained antitumor activity and improved control of minimal residual disease in preclinical leukemia models [75]. These findings indicate that progenitor-stage NK products may overcome one of the major limitations of mature NK cell therapies, namely their limited persistence following infusion. The iNKP platform was enabled by a developmental organoid-based differentiation strategy[76], further highlighting the therapeutic potential of harnessing immature NK cell lineage states rather than exclusively pursuing terminal maturation. In this context, the immature features observed in our iNK cell populations may provide opportunities for future optimization aimed at balancing persistence, developmental plasticity, and effector function.

In parallel, leveraging CAR engineering directly at the iPSC stage, previously constrained to a single modification in primary cells, could enable multi-modal engineering such as anti-CD19 CAR, non-cleavable CD16, IL-15/IL-15R fusion [70]. Such strategies could also be adapted to modulate NK cell effector functions implicated in pathological settings, including selective attenuation of ADCC or targeted depletion of pathogenic NK cell subsets, as suggested by recent success with CD38-targeting therapies in chronic AMR. When combined with scalable suspension manufacturing, offering a promising route for next-generation NK cell-based immunotherapies.

Together, these findings establish a unified, continuous, scalable, and standardized manufacturing framework for iPSC-derived NK cells. The hemanoid platform combines long-term hematopoietic progenitor maintenance with efficient NK cell lineage specification, achieving yields and consistency compatible with clinical translation. Future efforts should focus on enhancing late-stage maturation (KIR acquisition and adaptive NK formation), incorporating genetic engineering strategies (e.g., CARs or cytokine-secreting modules), and validating *in vivo* persistence. By bridging organoid biology with scalable bioprocess engineering, this system represents a significant step towards the mass production of standardized iNK cell products for future immunotherapy strategies.

Supplementary Material

Supplementary figures.
https://www.thno.org/v17p0551s1.pdf

Acknowledgments

The authors thank Dr. Matthias Ballmaier (Cell Sorting Facility, Hannover Medical School) and Dr. Oliver Dittrich-Breiholz and Team (Core Unit Transcriptomic, Hannover Medical School), and Ms. Sarina Lukis for their excellent scientific and technical support.

Funding

This work was supported by the Deutscher Akademischer Austauschdienst (DAAD) Graduate School Scholarship programme (FS57516591) to FS, Additional funding was provided by the German Center of Lung Research (DZL) to NL. This project has received funding from the European Research Council (ERC) under the European Union's Horizon 2020 research and innovation program (grant agreement No. 852178) (grant agreement No. 101100859 "iPYRO" and No. 101158172 "iMAClung). The views and opinions expressed are, however, those of the authors only and do not necessarily reflect those of the EU or the ERC. Neither the EU nor the granting authority can be held responsible for them. The work is also funded by the Deutsche Forschungsgemeinschaft (DFG, German Research Foundation) under Germany's Excellence Strategy -EXC 2155 -project number 390874280 and REBIRTH Research Center for Translational Regenerative Medicine "Förderung aus Mitteln des Niedersächsischen Vorab" (grant: ZN3340). The work is also funded by the Deutsche Forschungsgemeinschaft (DFG, German Research Foundation) LA 3680/9-1 and LA 3680/10-1. NL was also funded by zukunft.niedersachsen (Federal State of Lower Saxony), R2N.Micro-Replace-Systems. The Fraunhofer Internal Programs under Grant 533 No. Attract 40-01696. E.V. lab at CIML is funded by the by the European Research Council (ERC) under the European Union's Horizon (Treatlivmets, grant agreement no. 101118936), MSDAvenir, Innate Pharma, and institutional grants awarded to the CIML (INSERM, CNRS and Aix-Marseille University). E.V. is "Natural Killer Cells" Chair, Foundation Gustave Roussy. AB was supported by the nextGENERATION Medical Scientist Program funded by Else Kröner-Fresenius Foundation (2022_EKMK.13; to AB). The study was supported by grants from the Deutsche Forschungsgemeinschaft (DFG, German Research Foundation) Germany's Excellence Strategy-EXC 2155 "RESIST" Project number 390874280 (R.F.) and DFG Grant FO334/7-2 (FOR 2830-P6 to R.F.).

Author contributions

Conceptualization: FS and NL; Methodology: FS, LR, RJ, AB, BC, EEV, AM, RF, BEV, GM, SG, SB, DS, DC, MCO, CF, ACJ, GH, EV, and NL; Investigation: FS, and NL; Writing – Original Draft: FS; Writing – Review & Editing FS, LR, RJ, AB, BC, EEV, AM, RF, BEV, GM, SG, SB, DS, DC, MCO, CF, ACJ, GH, EV, and NL, Visualization: FS and NL. Project Administration: FS and NL; Funding Acquisition: FS and NL.

AI usage statement

The authors acknowledge the use of ChatGPT in the revision of this manuscript. AI assistance was used for language editing of the manuscript text. All scientific content, data interpretation, experimental design, and conclusions were reviewed, revised, and approved by the authors. No AI tools were used for data collection, statistical analysis, or image generation.

Data availability

The raw data of this study are available from the corresponding author upon reasonable request.

Ethics approval and consent to participate

Generation of the GMP line LiPSC-GR1.1 was supported by the NIH Common Fund Regenerative Medicine Program and reported in Stem Cell Reports. The NIH Common Fund and the National Center for Advancing Translational Sciences (NCATS) are joint stewards of the LiPSC-GR1.1 resource. (https://hpscreg.eu/cell-line/RUCDRi002-A)[77].

All patient samples, or their next of kin, provided full informed consent. Experiments were approved by the Local Ethics Committee in accordance with the world medical association's international code of ethics (10351_B0_K_2022).

Consent for publication

All consent and approval were taken from all authors and & co-authors.

Competing Interests

N.L. is an authors of the patent application (European patent application number PCT/EP2018/061574) entitled 'Stem-cell derived myeloid cells, generation and use thereof'. The priority date of the application is 4 May 2017.

All other authors declare no competing interests.

References

1. Kiessling R, Klein E, Pross H, Wigzell H. "Natural" killer cells in the mouse. II. Cytotoxic cells with specificity for mouse Moloney leukemia cells. Characteristics of the killer cell. Eur J Immunol. 1975; 5: 117-21.

2. Welsh RM, Jr. Cytotoxic cells induced during lymphocytic choriomeningitis virus infection of mice. I. Characterization of natural killer cell induction. J Exp Med. 1978; 148: 163-81.
3. Herberman RB, Nunn ME, Lavrin DH. Natural cytotoxic reactivity of mouse lymphoid cells against syngeneic acid allogeneic tumors. I. Distribution of reactivity and specificity. Int J Cancer. 1975; 16: 216-29.
4. Kobayashi M, Fitz L, Ryan M, Hewick RM, Clark SC, Chan S, et al. Identification and purification of natural killer cell stimulatory factor (NKSF), a cytokine with multiple biologic effects on human lymphocytes. J Exp Med. 1989; 170: 827-45.
5. Chiossone L, Dumas PY, Vienne M, Vivier E. Natural killer cells and other innate lymphoid cells in cancer. Nat Rev Immunol. 2018; 18: 671-88.
6. Vivier E, Tomasello E, Baratin M, Walzer T, Ugolini S. Functions of natural killer cells. Nat Immunol. 2008; 9: 503-10.
7. Park H, Kim G, Kim N, Ha S, Yim H. Efficacy and safety of natural killer cell therapy in patients with solid tumors: a systematic review and meta-analysis. Front Immunol. 2024; 15: 1454427.
8. Page A, Chuvin N, Valladeau-Guilemond J, Depil S. Development of NK cell-based cancer immunotherapies through receptor engineering. Cell Mol Immunol. 2024; 21: 315-31.
9. Kirkeby A, Main H, Carpenter M. Pluripotent stem-cell-derived therapies in clinical trial: A 2025 update. Cell Stem Cell. 2025; 32: 10-37.
10. Karre K, Ljunggren HG, Piontek G, Kiessling R. Selective rejection of H-2-deficient lymphoma variants suggests alternative immune defence strategy. Nature. 1986; 319: 675-8.
11. Karlhofer FM, Ribaudo RK, Yokoyama WM. MHC class I alloantigen specificity of Ly-49+ IL-2-activated natural killer cells. Nature. 1992; 358: 66-70.
12. Kim S, Poursine-Laurent J, Truscott SM, Lybarger L, Song YJ, Yang L, et al. Licensing of natural killer cells by host major histocompatibility complex class I molecules. Nature. 2005; 436: 709-13.
13. Boudreau JE, Hsu KC. Natural killer cell education in human health and disease. Curr Opin Immunol. 2018; 50: 102-11.
14. Laskowski TJ, Biederstadt A, Rezvani K. Natural killer cells in antitumour adoptive cell immunotherapy. Nat Rev Cancer. 2022; 22: 557-75.
15. Pirsadeghi A, Namakkoobi N, Behzadi MS, Pourzinolabedin H, Askari F, Shahabinejad E, et al. Therapeutic approaches of cell therapy based on stem cells and terminally differentiated cells: Potential and effectiveness. Cells Dev. 2024; 177: 203904.
16. Takahashi K, Yamanaka S. Induction of pluripotent stem cells from mouse embryonic and adult fibroblast cultures by defined factors. Cell. 2006; 126: 663-76.
17. Saleh F. Xeno-free cultivation of human induced pluripotent stem cells for clinical applications. 2021.
18. Karagiannis P, Takahashi K, Saito M, Yoshida Y, Okita K, Watanabe A, et al. Induced Pluripotent Stem Cells and Their Use in Human Models of Disease and Development. Physiol Rev. 2019; 99: 79-114.
19. Manstein F, Ullmann K, Kropp C, Halloin C, Triebert W, Franke A, et al. High density bioprocessing of human pluripotent stem cells by metabolic control and in silico modeling. Stem Cells Transl Med. 2021; 10: 1063-80.
20. Cuesta-Gomez N, Verhoeff K, Dadheech N, Dang T, Jasra IT, de Leon MB, et al. Suspension culture improves iPSC expansion and pluripotency phenotype. Stem Cell Res Ther. 2023; 14: 154.
21. Ackermann M, Haake K, Kempf H, Kaschutnig P, Weiss AC, Nguyen AHH, et al. A 3D iPSC-differentiation model identifies interleukin-3 as a regulator of early human hematopoietic specification. Haematologica. 2021; 106: 1354-67.
22. Dardano M, Kleemiss F, Kosanke M, Lang D, Wilson L, Franke A, et al. Blood-generating heart-forming organoids recapitulate co-development of the human haematopoietic system and the embryonic heart. Nat Cell Biol. 2024; 26: 1984-96.
23. Frenz-Wiessner S, Fairley SD, Buser M, Goek I, Salewskij K, Jonsson G, et al. Generation of complex bone marrow organoids from human induced pluripotent stem cells. Nat Methods. 2024; 21: 868-81.
24. Alsinet C, Primo MN, Lorenzi V, Bello E, Kelava I, Jones CP, et al. Robust temporal map of human in vitro myelopoiesis using single-cell genomics. Nat Commun. 2022; 13: 2885.
25. Ng ES, Sarila G, Li JY, Edirisinghe HS, Saxena R, Sun S, et al. Long-term engrafting multilineage hematopoietic cells differentiated from human induced pluripotent stem cells. Nat Biotechnol. 2024.
26. Euchner J, Sprissler J, Cathomen T, Furst D, Schrezenmeier H, Debatin KM, et al. Natural Killer Cells Generated From Human Induced Pluripotent Stem Cells Mature to CD56(bright)CD16(+)NKp80(+/-)In-Vitro and Express KIR2DL2/DL3 and KIR3DL1. Front Immunol. 2021; 12: 640672.
27. Wei X, Su C, Liu Y, Wei N, Xiang K, Qian Q, Xu Z. IPSC-derived NK cells for immunotherapy and therapeutic perspective (Review). Mol Med Rep. 2025; 32.
28. Strati P, Castro J, Goodman A, Bachanova V, Kamdar M, Awan FT, et al. Off-the-shelf induced pluripotent stem-cell-derived natural killer-cell therapy in relapsed or refractory B-cell lymphoma: a multicentre, open-label, phase 1 study. Lancet Haematol. 2025; 12: e505-e15.
29. Maartens JH, De-Juan-Pardo E, Wunner FM, Simula A, Voelcker NH, Barry SC, Hutmacher DW. Challenges and opportunities in the manufacture and expansion of cells for therapy. Expert Opin Biol Ther. 2017; 17: 1221-33.
30. Saleh F, Valdivia Malqui EE, Gensch I, Schinke M, Kappelhoj M, Nikolouli E, et al. Harnessing intermediate-scale bioreactors for next-generation macrophage production and application. Nat Protoc. 2026.
31. Ackermann M, Saleh F, Abdin SM, Rafiei Hashtchin A, Gensch I, Golgath J, et al. Standardized generation of human iPSC-derived hematopoietic organoids and macrophages utilizing a benchtop bioreactor platform under fully defined conditions. Stem Cell Res Ther. 2024; 15: 171.
32. Lachmann N, Ackermann M, Frenzel E, Liebhaber S, Brennig S, Happle C, et al. Large-scale hematopoietic differentiation of human induced pluripotent stem cells provides granulocytes or macrophages for cell replacement therapies. Stem Cell Reports. 2015; 4: 282-96.
33. Baghbaderani BA, Tian X, Neo BH, Burkall A, Dimezzo T, Sierra G, et al. cGMP-Manufactured Human Induced Pluripotent Stem Cells Are Available for Pre-clinical and Clinical Applications. Stem Cell Reports. 2015; 5: 647-59.
34. Chen G, Gulbranson DR, Hou Z, Bolin JM, Ruotti V, Probasco MD, et al. Chemically defined conditions for human iPSC derivation and culture. Nat Methods. 2011; 8: 424-9.
35. Knorr DA, Ni Z, Hermanson D, Hexum MK, Bendzick L, Cooper LJ, et al. Clinical-scale derivation of natural killer cells from human pluripotent stem cells for cancer therapy. Stem Cells Transl Med. 2013; 2: 274-83.
36. Muller C, Tufa DM, Chatterjee D, Muhlradt PF, Schmidt RE, Jacobs R. The TLR-2/TLR-6 agonist macrophage-activating lipopeptide-2 augments human NK cell cytotoxicity when PGE2 production by monocytes is inhibited by a COX-2 blocker. Cancer Immunol Immunother. 2015; 64: 1175-84.
37. Bryant J, Day R, Whiteside TL, Herberman RB. Calculation of lytic units for the expression of cell-mediated cytotoxicity. J Immunol Methods. 1992; 146: 91-103.
38. Chatterjee D, Marquardt N, Tufa DM, Beauclair G, Low HZ, Hatlapatka T, et al. Role of gamma-secretase in human umbilical-cord derived mesenchymal stem cell mediated suppression of NK cell cytotoxicity. Cell Commun Signal. 2014; 12: 63.
39. Crinier A, Dumas PY, Escaliere B, Piperoglou C, Gil L, Villacreces A, et al. Single-cell profiling reveals the trajectories of natural killer cell differentiation in bone marrow and a stress signature induced by acute myeloid leukemia. Cell Mol Immunol. 2021; 18: 1290-304.
40. Crinier A, Milpied P, Escaliere B, Piperoglou C, Galluso J, Balsamo A, et al. High-Dimensional Single-Cell Analysis Identifies Organ-Specific Signatures and Conserved NK Cell Subsets in Humans and Mice. Immunity. 2018; 49: 971-86 e5.
41. Foltz JA, Tran J, Wong P, Fan C, Schmidt E, Fisk B, et al. Cytokines drive the formation of memory-like NK cell subsets via epigenetic rewiring and transcriptional regulation. Sci Immunol. 2024; 9: eadk4893.
42. Aran D, Looney AP, Liu L, Wu E, Fong V, Hsu A, et al. Reference-based analysis of lung single-cell sequencing reveals a transitional profibrotic macrophage. Nat Immunol. 2019; 20: 163-72.
43. Ackermann M, Rafiei Hashtchin A, Manstein F, Carvalho Oliveira M, Kempf H, Zweigerdt R, Lachmann N. Continuous human iPSC-macrophage mass production by suspension culture in stirred tank bioreactors. Nat Protoc. 2022; 17: 513-39.
44. Ackermann M, Kempf H, Hetzel M, Hesse C, Hashtchin AR, Brinkert K, et al. Bioreactor-based mass production of human iPSC-derived macrophages enables immunotherapies against bacterial airway infections. Nat Commun. 2018; 9: 5088.
45. Lanier LL, Testi R, Bindl J, Phillips JH. Identity of Leu-19 (CD56) leukocyte differentiation antigen and neural cell adhesion molecule. J Exp Med. 1989; 169: 2233-8.
46. Cooper MA, Fehniger TA, Caligiuri MA. The biology of human natural killer-cell subsets. Trends Immunol. 2001; 22: 633-40.
47. Oetjen KA, Lindblad KE, Goswami M, Gui G, Dagur PK, Lai C, et al. Human bone marrow assessment by single-cell RNA sequencing, mass cytometry, and flow cytometry. JCI Insight. 2018; 3.
48. Granja JM, Klemm S, McGinnis LM, Kathiria AS, Mezger A, Corces MR, et al. Single-cell multiomic analysis identifies regulatory programs in mixed-phenotype acute leukemia. Nat Biotechnol. 2019; 37: 1458-65.
49. Li1 B, Kowalczyk1 MS, Slyper1 M, Jellert1 G, Tabaka1 M, Ashenberg1 O, et al. A single cell immune cell atlas of human hematopoietic system.
50. Hao Y, Hao S, Andersen-Nissen E, Mauck WM, 3rd, Zheng S, Butler A, et al. Integrated analysis of multimodal single-cell data. Cell. 2021; 184: 3573-87 e29.
51. Rebuffet L, Melsen JE, Escaliere B, Basurto-Lozada D, Bhandoola A, Bjorkstrom NK, et al. High-dimensional single-cell analysis of human natural killer cell heterogeneity. Nat Immunol. 2024; 25: 1474-88.
52. Poli A, Michel T, Theresine M, Andres E, Hentges F, Zimmer J. CD56bright natural killer (NK) cells: an important NK cell subset. Immunology. 2009; 126: 458-65.
53. Scott CL, Omilusik KD. ZEBs: Novel Players in Immune Cell Development and Function. Trends Immunol. 2019; 40: 431-46.
54. Thangaraj JL, Phan MT, Kweon S, Kim J, Lee JM, Hwang I, et al. Expansion of cytotoxic natural killer cells in multiple myeloma patients using K562 cells expressing OX40 ligand and membrane-bound IL-18 and IL-21. Cancer Immunol Immunother. 2022; 71: 613-25.
55. Phan MT, Lee SH, Kim SK, Cho D. Expansion of NK Cells Using Genetically Engineered K562 Feeder Cells. Methods Mol Biol. 2016; 1441: 167-74.
56. Woll PS, Martin CH, Miller JS, Kaufman DS. Human embryonic stem cell-derived NK cells acquire functional receptors and cytolytic activity. J Immunol. 2005; 175: 5095-103.
57. Imamura M, Shook D, Kamiya T, Shimasaki N, Chai SM, Coustan-Smith E, et al. Autonomous growth and increased cytotoxicity of natural killer cells expressing membrane-bound interleukin-15. Blood. 2014; 124: 1081-8.

58. Goldenson BH, Hor P, Kaufman DS. iPSC-Derived Natural Killer Cell Therapies - Expansion and Targeting. Front Immunol. 2022; 13: 841107.
59. Cooper MA, Elliott JM, Keyel PA, Yang L, Carrero JA, Yokoyama WM. Cytokine-induced memory-like natural killer cells. Proc Natl Acad Sci U S A. 2009; 106: 1915-9.
60. Romee R, Schneider SE, Leong JW, Chase JM, Keppel CR, Sullivan RP, et al. Cytokine activation induces human memory-like NK cells. Blood. 2012; 120: 4751-60.
61. Romee R, Rosario M, Berrien-Elliott MM, Wagner JA, Jewell BA, Schappe T, et al. Cytokine-induced memory-like natural killer cells exhibit enhanced responses against myeloid leukemia. Sci Transl Med. 2016; 8: 357ra123.
62. Shapiro RM, Birch GC, Hu G, Vergara Cadavid J, Nikiforow S, Baginska J, et al. Expansion, persistence, and efficacy of donor memory-like NK cells infused for posttransplant relapse. J Clin Invest. 2022; 132.
63. Fehniger TA, Shah MH, Turner MJ, VanDeusen JB, Whitman SP, Cooper MA, et al. Differential cytokine and chemokine gene expression by human NK cells following activation with IL-18 or IL-15 in combination with IL-12: implications for the innate immune response. J Immunol. 1999; 162: 4511-20.
64. Bjorkstrom NK, Riese P, Heuts F, Andersson S, Fauriat C, Ivarsson MA, et al. Expression patterns of NKG2A, KIR, and CD57 define a process of CD56dim NK-cell differentiation uncoupled from NK-cell education. Blood. 2010; 116: 3853-64.
65. Zhang L, Weiskittel TM, Zhu Y, Xue D, Zhang H, Shen Y, et al. Comparative dissection of transcriptional landscapes of human iPSC-NK differentiation and NK cell development. Life Med. 2024; 3: lnae032.
66. Yang C, Malarkannan S. Transcriptional Regulation of NK Cell Development by mTOR Complexes. Front Cell Dev Biol. 2020; 8: 566090.
67. Donnelly RP, Loftus RM, Keating SE, Liou KT, Biron CA, Gardiner CM, Finlay DK. mTORC1-dependent metabolic reprogramming is a prerequisite for NK cell effector function. J Immunol. 2014; 193: 4477-84.
68. Fallone L, Pouxvielh K, Arbez L, Rousseaux N, Picq L, Drouillard A, et al. Interleukins 15 and 18 synergistically prime the antitumor function of natural killer cells through noncanonical activation of mTORC1. Sci Signal. 2025; 18: eadq8778.
69. Biederstadt A, Rezvani K. Engineered natural killer cells for cancer therapy. Cancer Cell. 2025; 43: 1987-2013.
70. Ghobadi A, Bachanova V, Patel K, Park JH, Flinn I, Riedell PA, et al. Induced pluripotent stem-cell-derived CD19-directed chimeric antigen receptor natural killer cells in B-cell lymphoma: a phase 1, first-in-human trial. Lancet. 2025; 405: 127-36.
71. Broker K, Sinelnikov E, Gustavus D, Schumacher U, Portner R, Hoffmeister H, et al. Mass Production of Highly Active NK Cells for Cancer Immunotherapy in a GMP Conform Perfusion Bioreactor. Front Bioeng Biotechnol. 2019; 7: 194.
72. Goldenson BH, Zhu H, Wang YM, Heragu N, Bernareggi D, Ruiz-Cisneros A, et al. Umbilical Cord Blood and iPSC-Derived Natural Killer Cells Demonstrate Key Differences in Cytotoxic Activity and KIR Profiles. Front Immunol. 2020; 11: 561553.
73. Jacobs R, Hintzen G, Kemper A, Beul K, Kempf S, Behrens G, et al. CD56bright cells differ in their KIR repertoire and cytotoxic features from CD56dim NK cells. Eur J Immunol. 2001; 31: 3121-7.
74. Ding Y, Lavaert M, Grassmann S, Band VI, Chi L, Das A, et al. Distinct developmental pathways generate functionally distinct populations of natural killer cells. Nat Immunol. 2024; 25: 1183-92.
75. Wang Z, Zhang L, Huang D, Xia C, Weng Q, Lin Y, et al. Pluripotent stem cell-derived CAR-NK progenitor therapy targets minimal residual disease and prevents relapse in leukemia models. Cell Stem Cell. 2026; 33: 405-20 e6.
76. Huang D, Li J, Hu F, Xia C, Weng Q, Wang T, et al. Lateral plate mesoderm cell-based organoid system for NK cell regeneration from human pluripotent stem cells. Cell Discov. 2022; 8: 121.
77. Baghbaderani BA, Syama A, Sivapatham R, Pei Y, Mukherjee O, Fellner T, et al. Detailed Characterization of Human Induced Pluripotent Stem Cells Manufactured for Therapeutic Applications. Stem Cell Rev Rep. 2016; 12: 394-420.